

Facies-dependent $\delta^{13}\text{C}$ variation and diagenetic overprinting at the onset of the Sturtian glaciation in North-East Greenland

Robert M. Klæbe^a, et al.

Highlights

- Cryogenian base shown to be conformable based on primary sedimentological evidence
- New high-resolution $\delta^{13}\text{C}$ curve is presented
- Negative $\delta^{13}\text{C}$ values associated with carbonate precipitation from pore fluids
- Vertical shifts in $\delta^{13}\text{C}$ values linked to basin-wide sea level change
- Stratigraphic test of $\delta^{13}\text{C}$ reproducibility across the basin

For submission to *Precambrian Research* special issue

Facies-dependent $\delta^{13}\text{C}$ variation and diagenetic overprinting at the onset of the Sturtian glaciation in North-East Greenland

R. M. Klæbe^{a,1}, M. P. Smith^b, I. J. Fairchild^c, E. J. Fleming^d and M. J. Kennedy^e

^a *Sprigg Geobiology Centre, University of Adelaide, South Australia 5005, Australia*

^b *Oxford University Museum of Natural History, Parks Road, Oxford OX1 3PW, UK*

^c *School of Geography, Earth and Environmental Sciences, University of Birmingham, Birmingham B15 2TT, UK*

^d *CASP, University of Cambridge, Cambridge CB3 0DH, UK*

^e *Department of Earth and Planetary Sciences, Macquarie University, NSW 2109, Australia*

¹Corresponding author at Department of Geosciences and Natural Resource Management, Geology Section, University of Copenhagen, 1350 Denmark. E-mail address: rokl@ign.ku.dk

Abstract

Time-significant surfaces are used to construct a stratigraphic test of the intrabasinal reproducibility of a 16‰ Neoproterozoic carbon-isotope ($\delta^{13}\text{C}$) anomaly in the NE Greenland Caledonides. The $\delta^{13}\text{C}$ excursion from +6‰ to -10‰ occurs in the carbonate-dominated Andrée Land Group and lies below glacial diamictites of the Tillite Group commonly correlated as Sturtian in age (~720 Ma) and has been widely interpreted to record a global isotopic event reflecting a perturbation in the carbon cycle preceding the initiation of the snowball ice age. $\delta^{13}\text{C}$ stratigraphic patterns were determined in two strike sections with relatively shallow platform deposits at Kap Weber and slope deposits on Ella Ø preserved directly below the first evidence for glaciation. The top and bottom of the $\delta^{13}\text{C}$ profile was bounded by contiguous chronostratigraphic surfaces including an unconformity (sequence boundary) at the base recognisable in both sections and a subaerial exposure surface with a basinal correlative conformity at the top. The $\delta^{13}\text{C}$ profile at Kap Weber shows $\delta^{13}\text{C}$ values of +6‰ that drop to -8‰ in fine-grained slope deposits before returning to +6‰ in platform carbonates at the base of the glacial diamictite. The slope section on Ella Ø shows similar values for platform carbonates of +6‰ with a similar drop to ~-10‰ in slope deposits, but this section lacks the return to platform deposits evident at Kap Weber beneath the diamictite as well as a return to positive $\delta^{13}\text{C}$ values. The absence of the platformal sediments and positive $\delta^{13}\text{C}$ values on Ella Ø cannot be attributed to erosional truncation because the contact in this section shows a conformable, interbedded transition in to the glacial deposits indicating that a continuous record is preserved. This disparity in $\delta^{13}\text{C}$ values below the base of the Tillite Group suggests that the most negative $\delta^{13}\text{C}$ values recorded in slope mudstone facies (-10‰) occur near synchronously with values of +6‰ on the platform. Elemental mapping of the mudstone facies indicates that carbonate is largely pore-filling and authigenic, representing a secondary phase that is unlikely to record a seawater value. Elevated $\delta^{13}\text{C}$ values in shallow inner-ramp carbonate intervals may record locally modified seawater enriched in ^{13}C by photosynthesis and evaporation. The excursion in $\delta^{13}\text{C}$ values in the upper Andrée Land Group is therefore interpreted to result from a shift in facies from platform carbonates to carbonate cemented and diagenetically overprinted mudstone and does not record the secular change in seawater $\delta^{13}\text{C}$ used for correlation or interpretation of biogeochemical events preceding the snowball ice age.

Keywords: Neoproterozoic; Cryogenian; carbon isotopes; glaciation; authigenic carbonate

1. Introduction

Variations in carbon-isotope ($\delta^{13}\text{C}$) values recorded in sedimentary carbonate records are important for monitoring the Earth's carbon cycle through geologic time. Sharp declines in $\delta^{13}\text{C}$ values to as low as -10‰ in Neoproterozoic carbonate successions occur stratigraphically both below and immediately above diamictites interpreted to record globally synchronous ice ages (Fairchild and Kennedy, 2007; Hoffman et al., 1998; Kennedy et al., 1998; Sohl et al., 1999; Spence et al., 2016). The recurrence of this isotopic and stratigraphic motif across spatially isolated basins was used to establish a climatostratigraphic concept of globally synchronous pangu glaciation that is heralded by large-magnitude negative shifts in seawater $\delta^{13}\text{C}$, implying the onset of global glaciation was related to perturbations in the carbon cycle that were synchronously recorded by carbonate sediments as secular $\delta^{13}\text{C}$ variation (Hoffman et al., 1998; Schrag et al., 2002). However, the cause of these environmental changes and how $\delta^{13}\text{C}$ variation is related from section to section remains poorly understood because of limited physical stratigraphic and chemostratigraphic data at the appropriate resolution, and the scarcity of complete and independently correlated lateral sections. Further, erosion associated with glacial processes often results in an incomplete stratigraphic record locally or basin-wide that does not record a continuous series of depositional events.

Understanding how continuous the stratigraphic record is in pre-glacial sections, and the timing of $\delta^{13}\text{C}$ variation recorded within it in the context of local palaeoenvironmental changes, is critical in unravelling the role of changes in the global carbon cycle in triggering what are likely to have been the most severe climatic shifts in Earth history. The Neoproterozoic sequences exposed across the Caledonian fold belt in NE Greenland provide a natural laboratory where a stratigraphic framework can be established in order to determine the reproducibility of a routinely correlated $\delta^{13}\text{C}$ profile and the proposed relationship between secular change in seawater $\delta^{13}\text{C}$ (Hoffman et al., 2012; Knoll et al., 1986) and the onset of glaciation can be tested. This study examines the series of stratigraphic and isotopic events in lateral basinal sections across

the NE Greenland Caledonides that are commonly correlated to composite global $\delta^{13}\text{C}$ curves in order to investigate the precise timing relationship between $\delta^{13}\text{C}$ variation and the onset of glaciation.

2. The pre-Sturtian $\delta^{13}\text{C}$ Anomaly

A similar $\delta^{13}\text{C}$ profile and stratigraphic motif is reported in Neoproterozoic sequences of NE Greenland, Svalbard, Scotland and NW Canada where $\delta^{13}\text{C}$ values of $\sim +6\text{‰}$ in carbonate-bearing sediments abruptly decline to $\delta^{13}\text{C}$ values as low as -10‰ , which then locally recover to positive values of $+6$ to $+8\text{‰}$ (Brasier and Shields, 2000; Halverson et al., 2005; Halverson et al., 2004; Knoll et al., 1986; Macdonald et al., 2010; Prave et al., 2009). This positive-negative-positive feature in the Neoproterozoic $\delta^{13}\text{C}$ record in NE Greenland served as one of the key criteria used to support a Marinoan age for the associated overlying glaciogenic deposits (Halverson et al., 2004), until reinterpreted as Sturtian in age by Halverson et al. (2007) and Hoffman et al. (2012) based on comparison with distal sections in Svalbard interpreted to be intrabasinal correlatives. It is also a feature used to correlate Neoproterozoic $\delta^{13}\text{C}$ records from other basins (Halverson et al., 2005; Shields-Zhou et al., 2012). This correlation is based on 1) a common datum chosen as 0‰ that follows the $\delta^{13}\text{C}$ decline from relatively positive values of $\sim +6\text{‰}$ to negative values as low as -10‰ ; 2) a return to positive $\delta^{13}\text{C}$ values of up to $+8\text{‰}$ in some sections; and 3) an erosional sub-glacial surface related to the onset of a (contemporaneous) global ice age (Figure 1). In most sections from NW Canada and Svalbard the return to positive $\delta^{13}\text{C}$ values does not occur below glacial deposits (Halverson et al., 2004; Hoffman et al., 1998; Macdonald et al., 2010). Similarly, no significant $\delta^{13}\text{C}$ excursion is preserved in South Australia or Namibia in carbonate rocks that directly underlie interpreted Sturtian-aged diamictites. This disparity in pre-Sturtian glacial $\delta^{13}\text{C}$ records is interpreted to result from truncation by sub-glacial erosion that locally removed the upper portion of each isotopic profile. An alternative model for the pre-Sturtian $\delta^{13}\text{C}$ excursion in NE Greenland invokes chemical stratification of basin waters where contemporaneous $\delta^{13}\text{C}$ values decrease with increasing water depth (Fairchild et al., 2000). In this interpretation, stratigraphic variation in $\delta^{13}\text{C}$ values reflects sampling of this depth gradient rather than whole ocean secular variation.

3. The Andrée Land Group

The Cryogenian Andrée Land Group constitutes the upper portion of the Eleonore Bay Supergroup that crops out in a confined belt within the NE Greenland fjord region for over ~500 km N-S (Figure 2). Similar sedimentary sections in Scotland and Ireland (Brasier and Shields, 2000; Prave et al., 2009), and the Hecla Hoek succession in NE Svalbard (Fairchild and Hambrey, 1995; Harland, 1997), support the interpretation of a series of broad, shallow-water, connected cratonic basins that are associated with the onset of pre-lapetus extension and subsidence (Sønderholm et al., 2008 and references therein). The upper Andrée Land Group caps 12 km of dominantly siliciclastic shelf sedimentation and comprises the upper half of a ~2 km thick carbonate platform sequence. It is overlain by the ~900 m thick Tillite Group that comprises two discrete intervals of interpreted glaciogenic deposits, the Ulvesø and Storeelv Formations, which are separated by ~200 m of shales and sandstones of the fluvial Arena Formation (Fairchild and Hambrey, 1995). The Storeelv Formation is overlain by the non-glacial Canyon and Spiral Creek formations (Hoffman et al., 2012; Sønderholm et al., 2008), with a similar sequence occurring in sections from NE Svalbard (Fairchild et al., 2016).

The carbonates and fine-grained siliciclastics of the Andrée Land Group and the overlying deposits of the Tillite Group are well described in terms of the major lithostratigraphic and palaeoenvironmental transitions preserved (Fairchild and Hambrey, 1995; Fairchild et al., 2000; Frederiksen, 2000; Frederiksen, 2001; Hambrey and Spencer, 1987; Herrington 1989; Herrington and Fairchild, 1989; Moncrieff and Hambrey, 1990; Sønderholm et al., 2008). The Andrée Land Group lacks formal stratigraphic subdivisions, but was informally subdivided into 'bed-group' units 1-20 by Sønderholm and Tirsgaard (1993) that correspond to units AL1-7 of Frederiksen (2000). The present study deals with bed-groups 18-20 (AL5-7 respectively) and the interpreted glaciogenic Ulvesø Formation of the Tillite Group that were examined on Ella Ø and at Kap Weber (Figure 1).

Bed-group 18 records shallow carbonate ramp sedimentation characterised by microsparites with tepee and molar-tooth structures, channelised oolitic to pisolitic grainstones, and dolomitised intraclast packstones and stromatolitic biostromes (Frederiksen, 2000; Herrington and Fairchild, 1989, Figure 1). Following a regionally traceable interval of exposure, indicated by karstic dissolution and collapse breccias, upper bed-group 18 comprises a sequence of laminated microsparites that are interpreted as outer-ramp deposits. An abrupt change from ramp carbonates to deeper water, finer grained dolomitic silts and muds occurs near the base of bed-group 19. This unit comprises laterally continuous and interbedded fine-grained turbidites, laminated to massive mudstones, and carbonate-bearing clastic debris flows, that locally preserve isoclinal slump folds indicating slope to base-of-slope deposition. This relative rise in sea level is interpreted as tectonically forced and due to rapid basin subsidence that drowned the carbonate ramp in this region (Frederiksen, 2000; Sønderholm et al., 2008).

A return to shallow water ramp carbonates is recorded as bed-group 20, but is restricted to exposures in the north of the basin above an interpreted topographic high (Frederiksen, 2000; Hambrey and Spencer, 1987, Figure 1). In Ole Rømer Land and Andrée Land, the upper beds of bed-group 19 and lower beds of bed-group 20 are interbedded. Bed-group 20 shows an overall shallowing-upward trend from base-of-slope turbidites, interbedded outer-ramp mudstone and limestone couplets and turbidites, and to pisolitic limestones similar to those of lower bed-group 18. At both levels (bed-groups 18 and 20) ramp carbonates are inferred to have accumulated on a shallowly-dipping bank top with laterally extensive facies belts, although bed-group 20 reaches a maximum stratigraphic thickness of 240 m and wedges out towards the south over > 90km laterally (Frederiksen 1998). An abrupt facies boundary from these ramp carbonates to cross-bedded quartz sandstones interpreted as aeolian in origin marks the base of the Ulvesø Formation (Tillite Group) at Kap Weber and other localities in the north of the basin. At Kap Weber, 10 m of wavy laminated sandstones with outsized clasts directly overly the aeolian sands, followed by ~30 m of massive to stratified clast-poor diamictite comprising almost exclusively limestone and dolostone clasts that preserve

striations and facets in a dolomite-rich sandy matrix (Hambrey and Spencer, 1987; Moncrieff and Hambrey, 1990).

Farther south, bed-group 20 is absent (Herrington and Fairchild, 1989). Instead, the fine-grained siliciclastics and carbonates of bed group 19 are directly overlain by massive diamictites and lack the ramp carbonates and aeolianites present in the Kap Weber section. Clasts within these diamictites in both regions at the base of the Ulvesø Formation are lithologically similar (Figure 1). The thickness of Ulvesø Formation diamictite beds approaches 200 m in the most southern sections (Hambrey and Spencer, 1987) compared to tens of metres at Kap Weber to the north, and they contain debris flows and syn-sedimentary slumps at multiple levels. The absence of bed-group 20 in pre-glacial stratigraphy in the south of the basin has been interpreted to have resulted from subglacial erosion (Hoffman et al., 2012) or as representing a facies transition with conformable contact between bed-group 19 and glacial sediments (Hambrey and Spencer, 1987) that is associated with the onset of ice-rafting. The N-S exposures across the NE Greenland Caledonides are considered to provide a stratigraphic cross-section near-parallel to the palaeoshelf margin (Tirsgaard and Sørenholm, 1997), but where relatively shallower conditions prevailed to the north at Kap Weber in comparison with Ella Ø prior to and during the deposition of the Ulvesø Formation.

4. The Andrée Land Group – Tillite Group transition

4.1 Bed-group 19 on Ella Ø

The transition from ramp carbonates in upper bed-group 18 through slope deposits of bed-group 19 and into the base of the Ulvesø Formation was examined in detail on Ella Ø. Here, bed-group 18 comprises ~600 m of repeatedly cyclic shallow-water limestones and dolostones (Figure 1c). Following ~20 m of laminated, scoured, neomorphosed dolomicrosparites with tepee and molar-tooth structures, lower bed-group 18 comprises 100 m of decimetre-scale cross-bedded, channelized, oolitic and pisolitic grainstones (Figure 3a), undifferentiated microsparites (Figure 3b), and minor intraformational carbonate conglomerates, that shallow through 10 m of dolomitised intraclastic packstones (Figure 3c) and are capped by a distinctive

~5 m thick unit of dolomitised stromatolitic biostromes (Figure 3d and 3e). Up to seven abbreviated cycles (5 to 10 m in thickness) follow this sequence, followed by a further 150 m-thick cycle. A distinctive marker-horizon caps the sequence of cyclic limestones and comprises laminated dolostones with abundant vugs, bedding-parallel sheet-cracks, and poorly-sorted tabular breccias, with void space filled with fibrous fringing cements and coarse dolospar (Figure 3f), of which 15 m is exposed on Ella Ø. The terminal unit of bed-group 18 and basal unit of bed-group 19 comprises approximately 200 m of neomorphosed, laminated, silty-limestones, only the lower interval of which are exposed on Ella Ø (Figure 1c). The upper surface of this unit is however exposed at Kap Weber and terminates with brecciated dolostones on Kap Weber (Herrington and Fairchild, 1989). The first mudstones of bed-group 19 occur directly above this surface.

In general, mudstones, siltstones and clastic debrites recorded in bed-group 19 are arranged as a series of shallowing-upward cycles (Figures 4a and 5). Cycle bases are dominantly non-calcareous to slightly calcareous mudstones, occurring as massive and locally laminated units (Figure 4b). Pyrite is common in mudstone facies, and occurs as framboids and isolated euhedral crystals that are both disseminated throughout the rock matrix and concentrated along individual horizons (Figure 6). Mudstones are interbedded with sharp-based dolomitic siltstones and mudstones up to 5 cm thick, preserving irregular couplets of parallel laminated quartz-feldspar siltstone and structureless dolomite, and occasionally basal current ripples and sub-millimetric mudflake conglomerates, consistent with Tde and Tcde Bouma divisions respectively (Figure 4c) and interpreted as distal turbidites resulting from platform-slope gravity flows. Distal turbidite beds increase in regularity towards the top of each cycle, where cycle tops comprise stacked distal turbidite facies exclusively for up to 10 m and which are abruptly overlain by mudstones (lacking evidence for sediment gravity flows) that form the base of the subsequent cycle. Further up-section, 0.5 to 2 m thick sharp-based laterally-thinning debrites that preserve coarse-sand to cobble-sized material are interbedded with mudstone and distal turbidite facies (Figure 4d). Debrites carry rounded or tabular-bladed limestone and dolostone fragments, occasionally arranged in clast-rosettes, or are irregular in shape with diffuse boundaries, that are suspended in dominantly sand-grade dolomite matrix sediment. These carbonate

debrites mark the first evidence of near-pure carbonate following basal flooding of the ramp near the base of bed-group 19 and are likely related to shedding of semi-lithified carbonates from the carbonate platform margins. Transported, already-mineralised, molar tooth fillings also occur at this interval. Debrites are abruptly capped by distal turbidites and massive dolo-mudstones, consistent with suspension settling following mass flows on the slope. The upper interval of bed-group 19 records an abrupt return to slightly calcareous laminated to massive mudstone deposition with abundant organic laminae and pyritic concretions, including discrete 1 to 3 cm thick beds of black shale. This facies lacks evidence for sediment gravity flows apparent lower in the succession and passes vertically into diamictites of the Ulvesø Formation.

On Ella Ø, the Ulvesø Formation comprises ~100 m of weakly stratified clast-poor diamictites, debris flow breccias and subordinate rhythmites. Diamictites preserve clasts of dolostone and limestone, with subordinate cherty limestone, quartzite and millimetric calcareous mudstone fragments. Limestone clasts are typically gravel to pebble size, vary from angular to rounded, show little to no preferred grain orientation, and often preserve oolitic and stromatolitic textures that are similar to the dominant lithofacies of bed-groups 18 and 20. Clasts are commonly striated and/or faceted. Sharp-based debris flow deposits are present at multiple levels as 1 to 2 m thick packages of clast-rich muddy diamictites that carry up to boulder-sized clasts and rip-ups of carbonate. These units either load underlying semi-lithified clast-poor sandy diamictites or have erosive bases that cut down into underlying diamictite units by up to 1 m. Rhythmites occur as laterally discontinuous horizons ~5 to 10 mm thick and often preserve discrete outsized clasts. Lenticular sheets up to 10 m in width of partially dolomitized limestone occur at multiple levels from the base of the Ulvesø Formation, and preserve heavily recrystallized millimetric spheroidal allochems. The margins of these lenticular bodies are often irregular with evidence of soft-sediment deformation. The Ulvesø Formation is overlain by dominantly fluvial sandstones and shales of the Arena Formation with no cap carbonate deposit preserved, although a cap carbonate sequence is preserved in marine sediments above interpreted correlative Sturtian-aged diamictites on Svalbard (Fairchild et al., 2016).

4.2 Description of the basal glacial contact on Ella Ø

The interval spanning the upper Andrée Land Group and lower Ulvesø Formation was studied in detail at three localities on Ella Ø (Figure 2b) to address whether a time-continuous transition exists between bed-group 19 mudstones and overlying glaciogenic deposits or if erosion resulted in a significant time break between the units. In two of these examples (the Tømmerbugt and Kløftelv sections) the contact was continuously exposed. This contact is characterised by the following observations:

- 1) Interbedding of mudstones in bed-group 19 and diamictites compositionally identical to the basal Ulvesø Formation was documented at Tømmerbugt 2 m below the contact (Figure 7a). Concave-up lenses of diamictite are 0.3 to 1 m in width with ~80% tan-weathering matrix material of sand-sized carbonate. Clasts comprise subrounded sand-pebble microsparites, oolitic and pisolitic carbonates, often replaced by chert, subangular often tabular sandstone up to 3 cm, subrounded sand-pebble dolostones, 0.1 to 0.5 cm angular (vein) quartz, and angular and often tabular mudstone clasts that are compositionally similar to the mudstone substrate (Figure 7b). The lenticular morphology of these beds is similar to that of slope-debrites that are interbedded with mudstones lower in bed-group 19 (Figure 4d), but the clast and matrix composition resembles that of the overlying Ulvesø Formation diamictites (Figure 7c and 7d) and is consistent with the redeposition of glacially-reworked sediment as debris flows.
- 2) At both Tømmerbugt and Kløftelv, dolomitic muds are incorporated within the lower ~ 5 m of Ulvesø Formation diamictite (Figure 7d). Muds typically occur as 5 to 15 cm stringers that are mineralogically and texturally similar to those of the uppermost beds of bed-group 19 mudstone. Their irregular morphologies and diffuse margins indicate entrainment of semi-lithified mud into basal diamictite mass flows.
- 3) At Kløftelv, the bed-group 19 - Ulvesø Formation transition is abrupt, and the boundary is marked by the presence of extensive soft sediment deformation in the form of mudstone injection and dewatering (large-scale flame structures) into the Ulvesø Formation, with detached stringers of mudstone in the diamictite, and the presence of ball and pillow structures in the underlying bed-group 19 mudstones

(Figures 7e and 7i). Together these indicate that the mud in bed-group 19 had not dewatered and was unlithified when loaded by overlying mass flows of the Kløftelv Formation, and are inconsistent with presence of an unconformity surface between the two units.

4) At Kløftelv, lenses of calcite-rich packstone occur within the lowest 15 m of the diamictite deposits. Lenticular bodies range from 10 cm to 10 m in width with sharp convex-up bases and flat to low angle concave-down tops (Figure 7f and 7g). The Kløftelv section is well exposed with no evidence of faulting, and thus tectonic juxtaposition of the carbonates with the diamictites can be excluded. The lenses are therefore of primary sedimentary origin and comprise matrix-supported intraclasts of calcite microspar and reworked sub-millimetric allochems (peloids) that have been heavily recrystallised to calcite spar with occasional dolomicrospar overgrowths (Figure 7h). Matrix material comprises a relatively clean mosaic of calcite microspar. Stringers of more typical diamictite incorporated at the base of limestone lenses indicate syn-depositional emplacement.

4.3 Carbon-isotope trends

350 new $\delta^{13}\text{C}$ and $\delta^{18}\text{O}$ analyses presented here from Kap Weber and Ella Ø are focused on the interval between bed-group 18 and the base of the Ulvesø Formation diamictites. They augment the previous chemostratigraphic framework of the upper Andrée Land Group (Fairchild et al., 2000; Knoll et al., 1986) with the goal of establishing the timing of the negative $\delta^{13}\text{C}$ excursion recorded on Ella Ø and Kap Weber within a stratigraphic framework constrained by regionally-traceable stratigraphic surfaces. A cross plot of $\delta^{13}\text{C}$ and $\delta^{18}\text{O}$ analyses illustrates a number of distinctive lithologically and stratigraphically constrained populations (Figure 8).

$\delta^{18}\text{O}$ values are predominantly in the range of -2‰ to -8‰ with no obvious systematic relationship with $\delta^{13}\text{C}$. $\delta^{18}\text{O}$ values as high as 0‰ approach values typical of modern marine carbonates and argue against pervasive resetting of all $\delta^{18}\text{O}$ values during burial. A greater fraction of $\delta^{18}\text{O}$ values < -5‰ are challenging to

explain under modern marine conditions, but are consistent with typical temperature-dependent offsets during burial and stabilisation (Banner and Hanson, 1990).

$\delta^{13}\text{C}$ values show a wide range from +8‰ to -10‰, with values associated with specific stratigraphic intervals and host lithology. Ramp carbonates of bed-group 18 and bed-group 20 exclusively record positive $\delta^{13}\text{C}$ values that are commonly on the order of +6‰ to +8‰, reaching minimum values of +2‰ close to the major facies transition from outer ramp carbonates to slope mudstones near the base of bed-group 19 on Ella Ø and on Kap Weber. These positive values are recorded in calcitic and dolomitic microsparry grainstones, packstones and microbial facies (Figure 3), and are typically > 98% carbonate. In bed-group 18, a distinctive vertical stratigraphic shift and recovery of $\delta^{13}\text{C}$ values (150 m to 210 m, Figure 1c) from +5‰ to +2‰, recovering to +8‰, occurs along a flooding and subsequent shoaling cycle, with the 6‰ increase in $\delta^{13}\text{C}$ occurring within dominantly microbial dolostones and minimum values of +2‰ associated with pisolitic limestones. At the base of bed-group 20 on Kap Weber, similar $\delta^{13}\text{C}$ values in outer-ramp limestones record a steep increase over ~10 m from +2‰ to +7‰, with high values maintained until the overlying sequence boundary and aeolian transition at the base of the Ulvesø Formation (Figure 1b).

Bed-group 19 mudstones on Ella Ø record a range of $\delta^{13}\text{C}$ values from -3‰ to -10‰ (Figure 8) that scatter by up to 7‰ from bed to bed (Figure 1). This range is maintained throughout the mudstone facies (~10% to 25% carbonate) and distal turbidite facies (up to 95% carbonate) to the base of the Ulvesø Formation on Ella Ø and the onset of carbonate ramp deposition in bed-group 20 on Kap Weber. Carbonate debris flow material that is interbedded with mudstone and distal turbidite facies (Figure 4d) shares similar low values of -2.5‰ to -8‰ both in clast and matrix spot-samples (Figure 8), although most values are > -5‰. Circles that plot between +2‰ and -1‰ (Figure 8) are terminal outer-ramp limestones at the base of bed-group 19.

Clast and matrix material from Ulvesø Formation diamictites on Ella Ø were subsampled in an attempt to constrain the possible source of carbonate clasts and to test the timing of detrital reworking

compared to the emplacement of recorded $\delta^{13}\text{C}$ values. These data show good overlap with all local facies types developed in bed-group 18, 19 and 20, and show similar corresponding textures to these facies types in diamictite clasts. Spot-drilled matrix sub-samples record two ranges of $\delta^{13}\text{C}$ values: high values (+3.7‰ to +5.2‰) and low values (-4.2‰ to -5.3‰) that are isotopically similar to bed-group 18/20 platform carbonates and bed-group 19 dolomitic siliciclastics respectively. Carbonate clasts record a wide range of $\delta^{13}\text{C}$ values from -6.3‰ to +6.7‰, including two $\delta^{13}\text{C}$ values of ~0‰. All clasts with $\delta^{13}\text{C}$ values > 0‰ comprise limestone and dolostone and are texturally similar to local platform carbonates, while mudstone clasts exclusively record negative $\delta^{13}\text{C}$ values. The majority of carbonate lens material (Figure 7f) within the lower Ulvesø Formation has $\delta^{13}\text{C}$ values that fall within the range of -1.5‰ to +1.7‰, and comprise variable concentrations of microspar matrix carbonate and coarse sparry calcite and rhombic dolomite in recrystallised carbonate allochems (Figure 7h). The correlation between $\delta^{13}\text{C}$ values and clast/matrix lithology in basal Ulvesø Formation diamictites is consistent with these clastic deposits sampling the range of local facies types. This is consistent with the interpretation that Ulvesø Formation diamictites comprise ground-up carbonates derived from local carbonate platforms and slope deposits as diamictite matrix sediment and intraclasts. Limestone lenses (Figure 7f) that are shed from the platform margin as olistostromes record $\delta^{13}\text{C}$ values (0 ± 2 ‰) that are similar to values from carbonates in upper bed-group 18 and at the base of bed-group 19, and are also typical of modern seawater and pelagic carbonate values.

4.4 Mineral distribution

Platform deposits (bed-group 18 and 20) comprise carbonate allochems that have been recrystallised to calcite and dolomitic microspar, confirmed by thin section and hand-specimen examination. By contrast, interbedded mudstones and distal turbidites in bed-group 19 comprise variable mixtures of phyllosilicate clays, quartz, feldspars and micas, and a carbonate phase that comprises 15% to > 80% of the rock volume. Because the pre-Sturtian negative $\delta^{13}\text{C}$ excursion is defined by these mudstones, it is important to determine if the $\delta^{13}\text{C}$ values in this unit are a record of allochems that precipitated directly in the water

column, are derived from carbonate phases that post-date deposition and fill pores (cements), or comprise reworked grains swept from the eroding land surface or lithified carbonate platforms. Elemental mapping of representative mixed carbonate/siliciclastic samples from bed-group 19 demonstrates that the majority of carbonate preserved in bed-group 19 is dolomite (Figure 9 - 11). Across all examples of the mudstone facies examined (Figure 9, 10), > 90% of the carbonate volume in any given sample is well developed as coarse (> 10 μm) euhedral rhombic dolomite crystals, and < 4 μm angular dolomite grains (dolomicrite). By volume, coarse dolomite rhombs exceed dolomicrite (Figure 9b) and they occur in point-contact with adjacent siliciclastic grains. In unlaminated mudstones, dolomites are evenly distributed through the rock matrix, which is composed of > 50% clays previously reported as predominantly berthierine (Fairchild et al., 2000; Herrington and Fairchild, 1989), and ~30% subrounded to rounded quartz grains with subordinate feldspars and micas (< 10 μm in size). Detrital limestone grains (Figure 9b) are rare, well-rounded and < 4 μm in crystal size. Pyrite occurs evenly distributed as sub-micron euhedral crystals in association with clays, and as larger (aggregate) crystals < 5 μm in size. Mudstone beds that preserve laminae defined by clay versus quartz abundance (Figure 10) occasionally contain a further carbonate phase as mosaics of intergranular calcite. This calcite microspar occurs in relatively coarse mudstone-siltstone laminae and is cross-cut by quartz grains and dolomite rhombs (Figure 10e). The distribution and grain size of coarse dolomite crystals and calcite cements in these samples is independent of adjacent siliciclastic grain size (Figure 10b and 10c), while dolomicrite is more abundant in clay-rich horizons within laminated mudstones (Figure 10d).

Distal turbidite facies (Figure 11) preserve a similar mineralogy to mudstone facies, but erosive cycle bases are relatively quartz-rich and are typically 5-10 μm in grain size, with some grains up to 50 μm . Hemipelagic caps are dominantly clay in mineralogy and grain size. Dolomite in this facies is more abundant (> 50% of bulk) and varies in abundance depending on its position in an individual cycle. While siliciclastic minerals are well sorted between coarse cycle bases and hemipelagic caps, coarse dolomite crystals (> 10 μm in size) are ubiquitous regardless of cycle position (Figure 10b). Dolomite rhombs again range in size from micrite up to 20 μm , are most commonly > 10 μm , and are typically well-preserved angular rhombohedral

crystals. While siliciclastic grains are largely subrounded, relatively large dolomite crystals preserve sharp rhombohedral terminations in point-contact with siliciclastic grains. No carbonate allochems (ooids, peloids, carbonate intraclasts) or macro-scale microbial textures (microbial laminites, stromatolite domes) are identified in bed-group 19 mudstone or distal turbidite facies. The only allochems documented in bed-group 19 occur as intraclasts in carbonate debris flows that occur in the upper interval (Figure 4d). These are discrete lenses of allochthonous carbonate that moved down-slope as debris flows, likely from the platform margin, and contain semi-lithified clasts of limestone and dolostone.

5. Discussion

5.1 Relationship to relative sea-level

A comparison between the measured sections on Ella Ø and the correlative section at Kap Weber ~70 km north (Figure 1) reveals a common sequence of lithofacies changes that can be linked to basin-wide base level variation. The top surface of the brecciated dolostones near the base of bed-group 19 in both sections marks the first major landward translation of facies following ~2 km of lithologically similar carbonate ramp deposits (Herrington and Fairchild, 1989). This boundary records a flooding event of regional extent that drowned karstic surfaces on ramp carbonates of bed-group 18 and define a basal sequence boundary. Above this level, cyclic deposition of mudstones and siltstones (Figure 5) occurs in base-of-slope environments on both Ella Ø and Kap Weber, with two major 60 – 90 m cycles identified at each locality. A third cycle is identified on Ella Ø that includes interbedded mudstones and channelised carbonate breccias, which abruptly transition to a fourth cycle of organic-rich mudstones. This final cycle lacks interbedded debrites and distal turbidites and passes abruptly, but conformably (Figure 7), into Ulvesø Formation diamictites. In contrast, the third cycle identified on Kap Weber comprises a lower interval of carbonate-poor mudstones that are overlain by a ~100 m thick interval of laminated to wave-rippled microsparry limestones. A fourth cycle begins at a flooding surface marked by the return of carbonate-poor mudstones that again shoal into laminated and finally conglomeratic microsparry carbonates. At this level on Kap Weber,

limestones are sharply overlain by quartz sandstones, interpreted as aeolian (Moncrieff and Hambrey, 1990), that indicate a period of subaerial exposure and erosion associated with a significant basinward migration of the shoreline. A major transition of facies on Ella Ø also occurs at this level (the base of Ulvesø Formation) where organic carbonate-poor mudstones and minor black shale horizons are abruptly, but conformably, overlain by ~100 m of carbonate-bearing diamictite containing the first evidence of glacial reworking in the section. A correlative conformity along this interface is therefore inferred that corresponds to erosion along terminal ramp carbonates in the relatively shallow northern part of the basin at Kap Weber, and defines an upper sequence boundary. At Kap Weber, the first diagnostic evidence for glacial reworking of clasts does not occur until after a further flooding event that drowned aeolian sands and resulted in the deposition of ~10 m of wavy-laminated sandstones with outsized clasts and an overlying unit of diamictite that is lithologically and texturally similar to typical Ulvesø Formation diamictites described on Ella Ø.

The nature of cyclic deposition in bed-group 19 mudstone and siltstone intervals is challenging to associate with any single depositional process confidently. The number and thickness of major coarsening upward cycles between the Ella Ø and Kap Weber sections is consistent with an allocyclic forcing of the basin fill. On this basis, a tentative correlation of bed-group 19 cycles along inferred major flooding surfaces is indicated in Figure 12. However, the lateral continuity of sediment packages is difficult to resolve over distances > 1 km. The migration of local features such as submarine levees and channels that could have received relatively coarse-grained material shed from proximal platform environments cannot be discounted, and could indicate an autocyclical control that is localised. Regardless, the sequence boundaries identified near the base of bed-group 19 and the base of the Ulvesø Formation provide two significant stratigraphic surfaces between which the Ella Ø and Kap Weber sections can be compared.

The dominant matrix-supported poorly-stratified diamictites in the Ulvesø Formation are interpreted as waterlain rainout deposits where high sedimentation rates limited current reworking of sediment, with debris flows consistent with periodic instability on the slope and rhythmite horizons indicating

intervals of reduced sediment supply, interpreted as suspension deposits (Moncrieff and Hambrey, 1990). Previous workers have interpreted an extensive debris-laden ice shelf that shed significant volumes of coarse sediment into relatively shallow marine environments (Moncrieff and Hambrey, 1990). The similarity between carbonate diamictite clasts and the dominant lithofacies in the upper Andrée Land Group suggests that glaciogenic sediments originated from the erosion of landward and underlying carbonate platform and slope successions (Stouge et al., 2011). The emplacement of semi-lithified, shallow-water limestones as lenticular, olistostrome-type units at multiple levels within the Ulvesø Formation (Figure 7f and 7g) may suggest that carbonate production continued on local platforms that shed material whilst diamictites accumulated on the slope.

5.2 Stratigraphic Evolution

The proposed stratigraphic development for the Ella Ø and Kap Weber sections is summarised in Figure 13. This stratigraphic model relates the major facies transitions in the upper Andrée Land Group to the rise and fall of relative base-level across the platform, with the following sequence of events corresponding to panels a-i in Figure 13: a) Shallow-water platform carbonates are deposited under stable platform conditions. b) Exposure and sea-level fall causes regional karstification of laminated dolomicrite (Figure 3f), with a ~60 m thick unit occurring on Kap Weber and 15 m exposed on Ella Ø. c) Modest base-level rise superimposed outer ramp carbonates above this karst surface. d) The ramp was again exposed, indicated by erosion and brecciation at Kap Weber (Herrington and Fairchild, 1989). e) Following a period of non-deposition, a major marine transgression drowned ramp carbonates. This is accompanied by an abrupt change in facies to deep-water mudstones and interbedded distal turbidites that were likely shed from landward carbonate platforms and deposited by density currents in slope and toe-of-slope environments as the lower units of bed-group 19. f) Shoaling to outer ramp carbonates of bed-group 20 at Kap Weber, with relatively deeper water at Ella Ø, resulted in coarse clastic carbonate material shed from local platform margins accumulating as channel-scoured debris flows which were drowned by a subsequent sea-level rise

(Figure 13f). These debris flows were likely sourced from bed-group 20 equivalents, or from shoreward environments that continued carbonate precipitation. g) The onset of glacial conditions coincided with sea-level fall that resulted in exposure of the carbonate platform at Kap Weber while glacially reworked platform carbonates were deposited in the deeper regions of the basin (Ella Ø) as sediment gravity flows and via ice rafting resulting in massive to weakly-stratified diamictites. h) Pro-glacial aeolian sands were deposited on the exposed platform while glaciogenic deposition continued in the south of the basin. i) Subsequent flooding resulted in the landward migration of glacial outwash and deposition of weakly-stratified diamictites at Kap Weber above aeolian sands.

5.3 Origin of the ^{13}C -depleted carbonate in bed-group 19

The majority of carbonate that records the most negative values defining the pre-Sturtian glacial $\delta^{13}\text{C}$ excursion on Ella Ø is characteristically a rhombic dolomite phase in representative examples analysed from bed-group 19. Coarse dolomite crystals ($> 10\ \mu\text{m}$) are typically unsorted with respect to adjacent siliciclastic components that have undergone physical sorting through transport by density currents. Adjacent quartz grains are commonly subrounded to rounded and have a significantly finer grain size than coarse dolomite rhombs, despite these minerals being relatively resistant to physical weathering compared to dolomite. The euhedral crystal shape, sharp rhombic terminations, and point contact with adjacent siliciclastic grains are inconsistent with significant transport of these dolomite crystals. Further, in mudstone facies dolomite rhombs are disseminated throughout a matrix dominantly composed of clay minerals and are an order of magnitude larger in grain size. Similarly, dolomite crystal-size is relatively consistent regardless of its cycle position within distal turbidite beds (Figure 11) despite the differences in grain size but similarity in density of adjacent mixtures of siliciclastic grains. These features are difficult to explain if the $> 10\ \mu\text{m}$ dolomite phase is detrital and transported coeval with adjacent siliciclastic grains. The most parsimonious interpretation of this coarse dolomite phase invokes in situ formation of isolated rhombs, or rhombohedral overgrowth over detrital carbonate grains, within unlithified sediment that is comparable to

Phanerozoic examples of concretionary/cementing rhombic dolomite phases that are texturally similar (eg. Bojanowski, 2014; Hendry et al., 2000; Meister et al., 2006). Displacive dolomite precipitation likely occurred directly from pore fluids under shallow burial depths where the host sediment remained unlithified, allowing the growth of near-pristine dolomite rhombs.

Angular dolomite grains < 4 μm are subordinate to coarse dolomite rhombs by volume, and are disseminated throughout all samples examined, but are more common in clay-rich mudstone horizons (Figure 10d). These dolomicrites are in some cases sorted with adjacent siliciclastic materials (Figure 10b) and are often subangular to subrounded, consistent with detrital reworking and suspension settling. This material was likely transported in distal sediment gravity flows along with siliciclastic components on the slope, either as dolomite or as calcite and later replaced by dolomite in-situ, although evidence for partial dolomitisation of detrital limestone grains is not documented. Rare intergranular mosaics of calcite represent a further phase of carbonate deposition/precipitation, occurring as pore-filling cements that overgrow earlier dolomite rhombs and detrital quartz grains (Figure 10d and 10e). The $\delta^{13}\text{C}$ values defining the negative $\delta^{13}\text{C}$ excursion in the Andrée Land Group appear to record a mixed signal of early authigenic, detrital, and later diagenetic components. By volume, the authigenic rhombic dolomite phase contributed the most carbon to bulk $\delta^{13}\text{C}$ analyses.

5.4 Construction of the pre-Sturtian $\delta^{13}\text{C}$ excursion in NE Greenland

The sequence boundaries that bracket the bed-group 19/20 interval in the upper Andrée Land Group provide a pair of stratigraphic markers by which the stratigraphic and $\delta^{13}\text{C}$ records from Ella Ø and Kap Weber may be calibrated: 1) the subaerial exposure surface and abrupt facies transition from shallow carbonates to relatively deep-water clastic deposits near the base of bed-group 19 related to the abrupt drowning of the platform and 2) the erosion surface at the top of bed-group 20 (Kap Weber) that corresponds with the abrupt but conformable shift to diamictite deposition (Ella Ø). These surfaces allow the comparison and calibration of lateral basinal sections along physically correlated horizons that are independent of $\delta^{13}\text{C}$

values, providing a stratigraphic test of the synchronicity of $\delta^{13}\text{C}$ profiles across the basin. The sequence boundary at the base of bed-group 19 corresponds to a shift in $\delta^{13}\text{C}$ values from $\sim +6\text{‰}$ to negative values of -3‰ to -10‰ . This occurs both at Kap Weber and on Ella Ø and is preserved as a regionally traceable shift in lithofacies from relatively shallow-water ramp carbonates to slope mudstones and distal turbidites. The upper sequence boundary is defined differently between Kap Weber and Ella Ø, where the abrupt juxtaposition of aeolian sandstones above outer-ramp carbonates on Kap Weber records a sea-level fall that is synchronously expressed at Ella Ø by a rapid transition from homogeneous mudstone deposition to boulder-bearing diamictites.

Where a recovery from negative $\delta^{13}\text{C}$ values to values on the order of $+6\text{‰}$ occurs on Kap Weber along the lithofacies change back to ramp carbonates in bed-group 20, such a recovery is absent on Ella Ø. This presents a situation where the recorded $\delta^{13}\text{C}$ profile differs by up to 18‰ between Kap Weber and Ella Ø along a physically correlated stratigraphic surface. In this case, erosional truncation that has been suggested by previous workers to have occurred along the top of bed-group 19 on Ella Ø that removed the recovery of $\delta^{13}\text{C}$ values from -10‰ to $+6\text{‰}$ (Hoffman et al., 2012) is contradicted by primary sedimentological evidence. The only evidence of erosional truncation below the Ulvesø Formation occurs at Kap Weber below aeolian sandstones, contradicting previous interpretations that a more complete stratigraphic (and $\delta^{13}\text{C}$) record is preserved there in comparison to Ella Ø (Hoffman et al., 2012). Instead, the transition from slope mudstones to glacially reworked diamictite occurs gradually over several metres during which diamictite and mudstone deposition is coeval, illustrated by interbedding relationships, soft-sediment deformation, and incorporation of semi-lithified muds into diamictic mass flows at the base of the Ulvesø Formation (Figure 7). As such, the upper beds of the Andrée Land Group on Ella Ø likely retain the majority of their original depositional thickness and the sustained $\delta^{13}\text{C}$ values of -3‰ to -10‰ that are recorded by these sediments into the base of the Ulvesø Formation represent an uninterrupted isotopic record. This implies that the stratigraphic interval containing a return to positive $\delta^{13}\text{C}$ values that occurs at Kap Weber was not removed on Ella Ø but was never deposited.

5.5 Relative timing of basin fill and $\delta^{13}\text{C}$ variation

The bulk of preserved Precambrian carbonate occurs in general as recrystallised shallow-water allochems, microbially-mediated precipitates, and often reworked carbonate mud of ambiguous palaeoenvironmental origin. As such, the utility of $\delta^{13}\text{C}$ values derived from this record is supported primarily by the recurrence of similar vertical patterns between similarly-aged basins that are argued to record secular seawater variation that is equally recorded in all marine carbonate rocks. The stratigraphic model described here, coupled with petrographic evidence supporting a pore-fluid origin for the majority of carbonate in bed-group 19, illustrates that the negative $\delta^{13}\text{C}$ excursion from values of $\sim +6\text{‰}$ in bed-group 18 to values as low as -10‰ in bed-group 19 are unlikely to reflect a single changing seawater value. Instead, the negative $\delta^{13}\text{C}$ values in bed-group 19 that define the pre-Sturtian glacial $\delta^{13}\text{C}$ excursion in the upper Andr  e Land Group may have been recorded contemporaneously within the deeper areas of the basin or be entirely out of phase with platform carbonate deposition. The flooding of ramp environments near the base of bed-group 19 superimposed mudstones above shallow water carbonates as the carbonate factory migrated abruptly landward or shut down entirely due to increased sediment influx from the eroding land-surface. These slope and basin mudstones and distal turbidites accumulated mixtures of carbonate minerals as detrital grains and post-depositional cements, and record a wide range of negative $\delta^{13}\text{C}$ values in bulk samples.

Shallower conditions at Kap Weber allowed outer ramp limestones to prograde across bed-group 19 mudstones with sea-level fall or simply local differences in physical bathymetry. These carbonate deposits carried intermediate $\delta^{13}\text{C}$ values of $+2\text{‰}$ that quickly increased to $+7\text{‰}$ as the platform became increasingly established, and abruptly juxtaposed carbonate with high $\delta^{13}\text{C}$ values above mixed carbonate-siliciclastic slope deposits with negative $\delta^{13}\text{C}$ values in the north of the basin (Figure 14). Platform progradation at Kap Weber may have coincided with the appearance of coarse carbonate-bearing debris flows in middle to upper bed-group 19 on Ella    (Figure 4d) that are interbedded with mudstone and distal turbidite deposits. Evidence for soft-sediment deformation in carbonate-bearing debrites suggests that local carbonate

production resumed at least locally, and coeval with the deposition of detrital particles on the slope. On Ella Ø, $\delta^{13}\text{C}$ values remain negative into the base of the Ulvesø Formation, which is marked by channelised deposition of diamictite comprising of clasts of similar lithology to the ramp carbonates that occur lower in the succession. This abrupt but conformable transition on Ella Ø, a correlative conformity following the nomenclature of Van Wagoner et al. (1987), corresponds to the development of an erosional unconformity on Kap Weber that was shallow enough to expose ramp carbonates at sea-level lowstand. The observed vertical changes in $\delta^{13}\text{C}$ in the upper Andrée Land Group are thus controlled by variations in lithofacies that occur on spatial scales of tens of kilometres. Positive values are exclusively recorded by carbonate sediment that accumulated as allochems and microbial mats on shallow water bank tops while negative values are closely associated with deep-water pore fluid processes (Figure 8).

The lack of exposed deeper-basin and landward platform sections across the NE Greenland fjord region means that it is difficult to confirm whether pelagic mudstones and distal turbidites were deposited on the slope as condensed phases that correspond with synchronous carbonate-platform deposition. Alternatively, mudstone and turbidite deposition may be out of phase with platform carbonate deposition as increased siliciclastic deposition locally dominated over direct precipitation of carbonate allochems during sea-level highstand. The former interpretation is however consistent with sedimentological evidence that indicates the synchronous accumulation of siliciclastic and carbonate sediments within the basin, similar to correlative sections in Scotland (Fairchild et al., 2017). While inner ramp deposits (lower bed-group 18) contain few siliciclastic grains, outer ramp deposits in upper bed-group 18 and in bed-group 20 contain siliciclastic material that defines the laminae in millimetre-laminated silty limestones. Centimetre-scale ooids in decimetre-scale bedforms indicate relatively high energy of the inner ramp that would have led to the winnowing of clay and fine silt-sized particles. These particles were likely able to settle in relatively low-energy platform margins. Further, debris flows that carry carbonate clasts in middle to upper bed-group 19 show evidence of soft-sediment deformation as diffuse and irregular margins around carbonate intraclasts. Interbedding of semi-lithified near-pure carbonates in debris flows and slope mudstone deposits indicates

that direct carbonate precipitation continued locally up-slope while siliciclastics accumulated on the slope and in the basin. The absence of significant siliciclastic grains in the inner-ramp suggests that fine-grained detrital particles bypassed nearshore environments, perhaps by a combination of (low-volume) aeolian transport and winnowing in coastal wave-agitated waters, allowing carbonate production to continue while fine-grained siliciclastics accumulated on the slope. Alternatively, siliciclastic sediment may have moved longitudinally within the narrow basin from an external source and mixed with carbonate detritus that washed from platform margins, allowing bank-top carbonate precipitation to continue.

5.6 Causes of $\delta^{13}\text{C}$ variation in the upper Andrée Land Group

The dominant mechanisms driving carbonate precipitation between bed-group 18/20 and bed-group 19 are fundamentally different; precipitation of carbonate allochems, microbial mats and micrite directly from seawater, and dolomite precipitation from pore fluids respectively. Thus, the role of global secular changes in seawater $\delta^{13}\text{C}$ values versus the effects of local environmental effects and pore-scale processes is critical in correctly reading the $\delta^{13}\text{C}$ record of each sedimentary system. Positive $\delta^{13}\text{C}$ values of a similar magnitude and range to those recorded in bed-group 18 and 20 are common to most pre-Sturtian glacial carbonate successions, including the Ugab Subgroup in northern Namibia (+3‰ to +7‰, Halverson et al. 2002); the Fifteenmile, Tindir and Little Dal groups in northwestern Canada (+2‰ to +7‰, MacDonald et al. 2010); the Backlundtoppen and Elbobreen formations in northeastern Svalbard (+2‰ to +9‰, Halverson et al. 2007); and the Appin Group in western Scotland (+2‰ to +9‰, Prave et al. 2009, Fairchild et al. 2017). Secular changes in $\delta^{13}\text{C}$ values to > 5‰ have been linked to enhanced global rates of burial and storage of isotopically light carbon in the sedimentary record both as organic (Knoll et al., 1986) and inorganic phases (Schrage et al., 2013), resulting in ^{13}C -enriched seawater through much of the Neoproterozoic.

Interpreted within the conventional framework of secular seawater variation, the positive $\delta^{13}\text{C}$ values in bed-group 18 and 20 show the same range $\delta^{13}\text{C}$ values typical of the pre-Sturtian interval (Halverson et al., 2005). By excluding bed-group 19 as a local signal related to pore-fluid processes, $\delta^{13}\text{C}$ values in the

upper Andrée Land Group fluctuate smoothly between +3‰ and +8‰, showing a gradual decrease in younger outer-ramp carbonates at the top of bed-group 18 and the base of bed-group 19 to values of 0‰ to +4‰. Following a period of siliciclastic deposition, $\delta^{13}\text{C}$ values show the same range of +3‰ and +8‰ before truncation at the base of the Ulvesø Formation. Carbonate olistostromes in the Ulvesø Formation record younger carbonate that sampled falling $\delta^{13}\text{C}$ values of $0 \pm 2\text{‰}$. Under the interpretation of Schrag et al. (2013), negative $\delta^{13}\text{C}$ values recorded in bed-group 19 might sample the enhanced sink of authigenic carbonate invoked to buffer seawater $\delta^{13}\text{C}$ values to $> 5\text{‰}$.

Alternatively, the water-depth and facies dependence of $\delta^{13}\text{C}$ variation in the upper Andrée Land Group led Fairchild et al. (2000) to invoke basin-wide stratification of $\delta^{13}\text{C}$ values over whole-ocean secular change, where shallow bank-top carbonates sampled high $\delta^{13}\text{C}$ values from surface-water while deep-water facies sampled dissolved inorganic carbon (DIC) of ^{13}C -depleted bottom waters. Similar interpretations have since been offered for other Neoproterozoic units such as the Doushantuo Formation in southern China (Jiang et al., 2007; Li et al., 2017; Wang et al., 2017) and the Umberatana Group in the northwestern Adelaide geosyncline (Giddings and Wallace, 2009). A precedent for this type of depth-dependence of $\delta^{13}\text{C}$ values has since been set through detailed $\delta^{13}\text{C}$ investigations of modern carbonate-producing environments that need not invoke basin-wide chemical stratification or whole ocean secular change and represents a third possible interpretation of the positive $\delta^{13}\text{C}$ values recorded in bed-group 18 and 20 (e.g. Klæbe et al, 2017). Carbonate allochems and microbial mats that accumulate in modern shallow-marine environments routinely record positive $\delta^{13}\text{C}$ values up to +6‰. These anomalously high $\delta^{13}\text{C}$ values are recorded by sediments that mineralised synchronously with pelagic carbonates that accumulate in deep-ocean basins and record atmospheric equilibrium values of $\sim 0\text{‰}$. For example, maximum values of +5.5‰ and +4.5‰ are preserved in both skeletal and non-skeletal allochems on the modern Belize-Yucatan platform and Kuwait carbonate ramp respectively in surface sediment and drill core (Gischler and Lomando, 2005; Gischler et al., 2007), with the most positive values occurring in coastal oolitic sands. Similar values ranging from +4.5‰ to +6‰ occur in subtidal stromatolitic and algal-mat carbonates in Shark Bay, Western Australia, that are attributed to

locally enhanced microbial photosynthesis under evaporative and poorly-circulated waters (Jahnert and Collins, 2012). On the Great Bahama Bank, platform-top, non-skeletal, dominantly oolitic carbonate sands record positive $\delta^{13}\text{C}$ values up to +6‰ (Oehlert et al., 2012) that are locally modified by photosynthetic effects under poorly circulated marine waters < 6 m deep (Melim et al., 2001). In this example, $\delta^{13}\text{C}$ values decrease on the platform slope as platform-derived carbonate allochems (+4‰ to +6‰) proportionally mix with pelagic carbonate (~0‰) that sample well-mixed marine surface waters (Oehlert et al., 2012; Swart and Eberli, 2005).

The range of $\delta^{13}\text{C}$ values preserved in bed-group 18 and 20 platform sections (+2‰ to +8‰) largely falls within the range of $\delta^{13}\text{C}$ values that occur in modern platform carbonates (< +6‰). The most positive $\delta^{13}\text{C}$ values in bed-group 18 of +8‰ are recorded by shallow-water oolitic and dolomitised stromatolitic carbonates with evidence for subaerial exposure, karst formation, collapse, and re-deposition of locally-derived rip-up clasts. Lower values ($0 \pm 2\text{‰}$) are exclusively recorded by: 1) terminal outer-ramp carbonates at the base of bed-group 19 that are directly overlain by mudstones related to the drowning of the platform; 2) carbonate olistostromes preserved at multiple levels in the Ulvesø Formation; and 3) individual carbonate clasts in Ulvesø Formation diamictites (Figure 8). Near-marine (0‰) $\delta^{13}\text{C}$ values recorded by autochthonous outer-ramp carbonates and allochthonous olistostrome carbonates shed from the platform margin onto the slope indicate that $\delta^{13}\text{C}$ values varied along a depth-gradient from the inner-ramp to the platform margin. Fine-grained carbonate muds precipitated near the platform margin where DIC more closely resembled that of open-ocean waters while nearshore oolitic and pisolitic grainstone, and microbial carbonates, record heavy $\delta^{13}\text{C}$ values from shallow and restricted bank-top waters. This type of spatial gradient is analogous to Bahama Bank-type mixing of platform-top and pelagic carbonate beyond the platform margin where water depths exceed 10m (Oehlert et al., 2012; Swart and Eberli, 2005).

The lack of a smooth $\delta^{13}\text{C}$ curve in bed-group 19 suggests a more stochastic origin for negative $\delta^{13}\text{C}$ values of -3‰ to -10‰ than a single changing seawater value recorded by precipitating carbonate. $\delta^{13}\text{C}$

values in bed-group 19 mudstones and distal turbidites do not appear to change systematically along shallowing cycles in this interval (Figure 1), which might be predicted in a chemically stratified basin in which carbonate is precipitating directly from the water column along a depth-gradient. Bulk $\delta^{13}\text{C}$ values recorded in these samples are difficult to assign to any single process as they consist of a mixture of genetically different carbonate phases. Rather, the wide range of $\delta^{13}\text{C}$ values in bed-group 19, and the bed-to-bed scatter in values of up to 7‰, is consistent with bed-group 19 mudstones recording a variable mixture of carbon sources with different $\delta^{13}\text{C}$ values. The mudstone and distal turbidite facies contain multiple phases of carbonate, including detrital grains likely swept from eroding platforms and authigenic carbonate (the majority of which is dolomite) that precipitated in situ. Detrital carbonates occur as dolomicrite and, rarely, micritic calcite that is evenly distributed in massive mudstones but is greater in abundance within clay-rich horizons in laminated mudstones suggesting that these grains settled alongside hemipelagic clay particles under relatively deep water. The origin of these grains is ambiguous, but it is likely that they are supplied by the erosion of local lithified carbonate platforms or older regional carbonate rocks.

Detrital grains are dispersed with an authigenic rhombohedral dolomite phase that precipitated directly from pore fluids during early burial. This phase precipitated pre-compaction, supported by the euhedral rhombic morphology and apparent displacement of siliciclastic grains, similar to examples of concretionary dolomites from the Phanerozoic in terms of crystal size, habit and the distribution of dolomite versus adjacent siliciclastics. These authigenic dolomites are the most voluminous carbonate phase identified and are thus the most significant carbon source that influenced bulk $\delta^{13}\text{C}$ values. Negative $\delta^{13}\text{C}$ values in bed-group 19 might implicate bacterial sulphate reduction as a major source of isotopically-light carbon to marine pore fluids. Framboidal pyrite and organic matter are both common components of bed-group 19 siliciclastic sediment, consistent with the active reduction of dissolved sulphate that can result in the precipitation of authigenic dolomite in anoxic sediment directly from pore waters (Irwin et al., 1977). Carbonate-bearing debris flows in middle to upper bed-group 19 record $\delta^{13}\text{C}$ values are 2 to 3‰ higher than those recorded in

interbedded mudstones and distal turbidites and necessarily contain a significantly larger component of detrital carbonate but likely experienced some pore-fluid mixing with adjacent unlithified muds.

5.7 Chemostratigraphic utility of the pre-Sturtian $\delta^{13}\text{C}$ excursion in NE Greenland

Diagenetic cements are typically not used for inter- or intra-basinal correlation of $\delta^{13}\text{C}$ values as they often preserve local signals related to pore fluid processes or secondary overprints that are dissimilar from seawater values. However, recent authors have argued that diagenetic cements recording the Ediacaran ‘Shuram/Wonoka’ $\delta^{13}\text{C}$ excursion might retain some chemostratigraphic utility (Cui et al, 2017; Zhou et al, 2016), which is similar in its stratigraphic thickness and range of $\delta^{13}\text{C}$ values to the pre-Sturtian $\delta^{13}\text{C}$ excursion. In these examples, enhanced authigenic carbonate precipitation is interpreted to be linked with the increased sulphate concentrations in the Earth’s oceans as a function of atmospheric O_2 concentrations, driving the precipitation of authigenic carbonate via pore fluid sulphate reduction and anaerobic methane oxidation. While the pre-Sturtian $\delta^{13}\text{C}$ excursion in bed-group 19 occurs as variable negative $\delta^{13}\text{C}$ values in fine-grained organic-rich siliciclastic sediment that is likely to have hosted such reactions, sections from NE Svalbard and NW Canada interpreted to record the pre-Sturtian $\delta^{13}\text{C}$ excursion are dominated by organic-lean, coarse grained, shallow water carbonate allochems with evidence for subaerial exposure and karst (Halverson et al. 2005; Macdonald et al. 2010; Macdonald and Roots 2009). Platform-top precipitation of carbonate is expected to sample the $\delta^{13}\text{C}$ values of ambient surface water DIC, while precipitation via pore-fluid sulphate reduction liberates isotopically light carbon and generates alkalinity from organic matter in the sediment, and therefore the catalyst for carbonate precipitation and source of carbon in each example is fundamentally different. Further, platform-top carbonate allochems undergo a different set of diagenetic reactions (Knauth and Kennedy 2009) compared with deep-water, organic-rich siliciclastic sediments, which are not limited by marine sulphate concentrations. As there are no available independent age dates in the pre-Sturtian NE Greenland or NE Svalbard sections to confirm correlations, and the negative excursion occurs along a shallowing trend in NE Svalbard and NW Canada compared to a regional flooding event in NE Greenland, a

local diagenetic origin for the pre-Sturtian $\delta^{13}\text{C}$ excursion in NE Greenland that is not recording global processes appears to be the most consistent with the data at hand.

Under the basinal and diagenetic constraints discussed here, the linkage of glaciogenic sediment and negative $\delta^{13}\text{C}$ values in the upper Andr  e Land Group becomes convoluted. While negative $\delta^{13}\text{C}$ values likely represent discrete local signals rather than a progression of isotopic change in seawater DIC, a conformable transition between negative $\delta^{13}\text{C}$ values and the first glaciogenic sediment of the Ulves   Formation on Ella    does indicate that these processes are directly related in time. The fall in sea-level responsible for the formation of the sequence boundary at the base of the Ulves   Formation on Ella    appears to coincide with the onset of glacial conditions. Clasts within these deposits show striations and facets that identify physical reworking of carbonate grains by glacial processes rather than typical erosion and collapse of an exposed carbonate platform (Moncrieff and Hambrey, 1990). The first diagnostic evidence of glacial influences does not occur at Kap Weber until after aeolian sandstones at the base of the Ulves   Formation are flooded and deposition of marine siliciclastic sediments resumes (Figure 1). These laminated sandstones carry discrete outsized clasts interpreted to be related to ice-rafting, and are overlain by boulder-bearing diamictites similar to those that dominate the Ulves   Formation on Ella   . The contrast in stratigraphic sequences leading into glacially-influenced sedimentation between the northern and southern regions of the basin reflect the strong influence that local geomorphology had on the distribution of glacial sediment both laterally and through time. Conformity along the bed-group 19 – Ulves   Formation boundary coeval with pro-glacial aeolian deposition, and the subsequent flooding of the basin and accumulation of glacio-marine facies, is difficult to reconcile with a single period of ice build-up. Regardless, there is no clear connection between negative $\delta^{13}\text{C}$ values and causes of glaciation through the carbon cycle because these values largely represent pore scale processes and occur coeval with positive $\delta^{13}\text{C}$ values within the same basin.

6. Conclusions

1) This study demonstrates that a pre-Sturtian negative $\delta^{13}\text{C}$ stratigraphic excursion can be reconstructed as a feature corresponding with relative sea-level change in the basin. In the upper Andrée Land Group, positive $\delta^{13}\text{C}$ values are only recorded by shallow-water carbonate allochems in bed-group 18 and, in the north of the basin, in bed-group 20, while negative values occur in carbonate-bearing fine grained siliciclastic sediments in bed-group 19. Correlation of laterally equivalent sections using two regional tie-lines provide an independent test of the timing and reproducibility of $\delta^{13}\text{C}$ profiles between the relatively shallow north and deeper south of the basin and indicates that the negative $\delta^{13}\text{C}$ excursion occurs as the carbonate platform was drowned and relatively deep-water siliciclastic sediments were deposited, and locally recovers to positive $\delta^{13}\text{C}$ values where prograding platform carbonates overly these siliciclastic sediments. The base of the first glaciogenic deposits on Ella Ø is interpreted to be the correlative with erosion and aeolian sand deposition at Kap Weber as glacioeustatic sea level fall exposed shallow water carbonate platforms in the north of the basin, indicating that direct precipitation of carbonate with $\delta^{13}\text{C}$ values of $\sim +8\text{‰}$ was correlative and co-occurred with values as low as -10‰ on the slope.

2) A conformable boundary at the base of the Ulvesø Formation on Ella Ø confirms that the lateral difference in $\delta^{13}\text{C}$ patterns and lithology directly below Sturtian glaciogenic deposits in NE Greenland is a primary feature that is unrelated to erosional truncation. Instead, the change from $\delta^{13}\text{C}$ values of -10‰ to values of $+8\text{‰}$ in bed-group 20 at Kap Weber occurs as carbonate platforms are locally and conformably re-established in the relatively shallow north of the basin. No similar recovery in $\delta^{13}\text{C}$ values to $+8\text{‰}$ occurs on Ella Ø in the south where slope to base-of-slope deposition continued into the base of the first glaciogenic sediments of the Ulvesø Formation with no significant break in sedimentation.

3) Elemental mapping of bed-group 19 mudstones and distal turbidites identifies a mixture of carbonate phases, including fine-grained likely detrital dolomite and calcite, relatively coarse-grained rhombohedral dolomite, and later overgrowths of calcite. The observed association between displacive dolomite, framboidal pyrite, and organic matter, coupled with anomalous and variable $\delta^{13}\text{C}$ values as low as

-10‰, implicates the production of pore-fluid alkalinity and dissolved carbon via sulphate reduction as the dominant driver of authigenic carbonate precipitation in these rocks. This implies that the most significant carbonate phase by-volume that records pre-Sturtian $\delta^{13}\text{C}$ excursion in NE Greenland was precipitated during early diagenesis rather than directly from the water column. This phase thus records the $\delta^{13}\text{C}$ values of ambient pore-waters, which is determined by the input of carbon liberated from buried organic matter and not by carbon exchange with seawater. Regardless of the origin of the authigenic dolomite phase, the mixture of detrital and pore-fluid carbonate preserved here is not expected to have inter-basinal chemostratigraphic significance as it cannot be directly linked to global changes in $\delta^{13}\text{C}$ values of seawater. Further, ^{13}C -enriched carbonate is a common feature of modern shallow-water carbonate platforms where bank top circulation is limited and primary productivity is high, potentially explaining in-part the heavy $\delta^{13}\text{C}$ values measured in bed-group 18 and 20.

4) Although similar in shape and stratigraphic thickness to other $\delta^{13}\text{C}$ excursions in pre-Sturtian strata, the ~18‰ $\delta^{13}\text{C}$ excursion recorded in the Andrée Land Group in NE Greenland can simply be explained by the stacking of a series of transient depositional phases that record $\delta^{13}\text{C}$ values related to local palaeoenvironmental conditions and post-depositional processes rather than changing global seawater values. Where local geomorphology means that strike-sections periodically accumulated under significantly different palaeoenvironmental conditions that respond differently to changes in base-level, an entirely unique sequence of lithological transitions (and associated $\delta^{13}\text{C}$ values) is expected. While lithofacies are understood not to be coeval across an entire basin, sea-level forcing is synchronous in basins that are open to marine connections and thus provides a powerful tool in confirming or challenging chemostratigraphic correlations.

Acknowledgements

This work was supported by the Sprigg Geobiology Centre at the University of Adelaide, the University of Birmingham and the University of Oxford, and by ARC grants DP120100104, DP110104367 and LP120200086, NERC grant GR3/NE/H004963/1, and Australian Synchrotron beam-time (ref. AS133/XFM/7150 awarded to MJK). The Danish authorities are thanked for field permissions and the Cambridge Arctic Shelf Programme for extensive logistical support during field work in 2012. We thank S. Löhr, T. Hall, and P. Knauth for comments and discussion of this manuscript. R. Drysdale and M. Rollog are thanked for analytical support. We thank Jon Ineson and an anonymous reviewer for providing valuable feedback which improved this manuscript.

Supplementary data

Supplement containing raw stable isotope data can be found in the online version at:

References cited

- Banner, J.L., Hanson, G.N., 1990. Calculation of simultaneous isotopic and trace element variations during water-rock interaction with applications to carbonate diagenesis. *Geochimica et Cosmochimica Acta* 54, 3123-3137.
- Bojanowski, M.J., 2014. Authigenic dolomites in the Eocene–Oligocene organic carbon-rich shales from the Polish Outer Carpathians: Evidence of past gas production and possible gas hydrate formation in the Silesian basin. *Marine and Petroleum Geology* 51, 117-135.
- Cui, H., Kaufman, A.J., Xiao, S., Zhou, C., Liu, X.-M., 2017. Was the Ediacaran Shuram Excursion a globally synchronized early diagenetic event? Insights from methane-derived authigenic carbonates in the uppermost Doushantuo Formation, South China. *Chemical Geology* 450, 59-80
- Brasier, M.D., Shields, G., 2000. Neoproterozoic chemostratigraphy and correlation of the Port Askaig glaciation, Dalradian Supergroup of Scotland. *Journal of the Geological Society* 157, 909-914.
- Fairchild, I.J., Bonnand, P., Davies, T., Fleming, E.J., Grassineau, N., Halverson, G.P., Hambrey, M.J., McMillan, E.M., McKay, E., Parkinson, I.J., Stevenson, C.T.E., 2016. The Late Cryogenian Warm Interval, NE Svalbard: Chemostratigraphy and genesis. *Precambrian Research* 281, 128-154.
- Fairchild, I.J., Hambrey, M.J., 1995. Vendian basin evolution in East Greenland and NE Svalbard. *Precambrian Research* 73, 217-233.
- Fairchild, I.J., Kennedy, M.J., 2007. Neoproterozoic glaciation in the earth system. *Journal of the Geological Society* 164, 895-921.
- Fairchild, I.J., Spencer, A.M., Ali, D., Anderson, R.P., Anderton, R., Boomer, I., Dove, D., Evans, J.D., Hambrey, M.J., Howe, J., Sawaki, Y., Shields, G., Skelton, A., Tucker, M.E., Wang, Z., Zhou, Y., 2017. Tonian-Cryogenian boundary sections of Argyll, Scotland. *Precambrian Research*, doi: 10.1016/j.precamres.2017.09.020.
- Fairchild, I.J., Spiro, B., Herrington, P.M., 2000. Controls on Sr and C isotope compositions of Neoproterozoic Sr-rich limestones of East Greenland and North China, in: Grotzinger, J.P., James, N.P. (Eds.), *Carbonate Sedimentation and Diagenesis in an Evolving Precambrian World*, SEPM Special Publication 67, 297-313.
- Frederiksen, K.S., 2000. Evolution of a Late Proterozoic Carbonate Ramp (Ymer Ø and Andrée Land Groups, Eleonore Bay Supergroup, East Greenland): Response to Relative Sea-Level Rise. *Polarforschung* 68, 125-130.
- Frederiksen, K.S., 2001. A Neoproterozoic carbonate ramp and base-of-slope succession, the Andrée Land Group, Eleonore Bay Supergroup, North East Greenland: Sedimentary facies, stratigraphy and basin evolution. PhD Thesis. University of Copenhagen, Denmark.
- Giddings, J.A., Wallace, M.W., 2009. Facies-dependent [δ] ^{13}C variation from a Cryogenian platform margin, South Australia: Evidence for stratified Neoproterozoic oceans? *Palaeogeography, Palaeoclimatology, Palaeoecology* 271, 196-214.
- Gischler, E., Lomando, A.J., 2005. Offshore sedimentary facies of a modern carbonate ramp, Kuwait, northwestern Arabian-Persian Gulf. *Facies* 50, 443-462.
- Gischler, E., Swart, P.K., Lomando, A.J., 2007. Stable isotopes of carbon and oxygen in modern sediments of carbonate platforms, barrier reefs, atolls, and ramps: patterns and implications. *Perspectives in carbonate geology: a tribute to the career of Robert Nathan Ginsburg*, 61-74.
- Halverson, G.P., Hoffman, P.F., Schrag, D.P., Kaufman, A.J., 2002. A major perturbation of the carbon cycle before the Ghaub glaciation (Neoproterozoic) in Namibia: Prelude to snowball Earth? *Geochemistry Geophysics Geosystems* 3, 1-24.
- Halverson, G.P., Hoffman, P.F., Schrag, D.P., Maloof, A.C., Rice, A.H.N., 2005. Toward a Neoproterozoic composite carbon-isotope record. *Geological Society of America Bulletin* 117, 1181-1207.
- Halverson, G.P., Maloof, A.C., Hoffman, P.F., 2004. The Marinoan glaciation (Neoproterozoic) in northeast Svalbard. *Basin Research* 16, 297-324.

- Halverson, G.P., Maloof, A.C., Schrag, D.P., Dudas, F.O., Hurtgen, M., 2007. Stratigraphy and geochemistry of a ca 800 Ma negative carbon isotope interval in northeastern Svalbard. *Chemical Geology* 237, 5-27.
- Hambrey, M.J., Spencer, A.M., 1987. Late Precambrian glaciation of central east Greenland. *Meddelelser om Grønland* 19, 50.
- Harland, W.B., 1997. The Geology of Svalbard. Geological Society London, Memoirs 17, 110-131.
- Hendry, J.P., Wilkinson, M., Fallick, A.E., Trewin, N.H., 2000. Disseminated 'jigsaw piece' dolomite in Upper Jurassic shelf sandstones, Central North Sea: an example of cement growth during bioturbation? *Sedimentology* 47, 631-644.
- Herrington, P.M., 1989. Stratigraphy, sedimentology and diagenesis of late Precambrian carbonates from the upper limestone-dolomite "series", central East Greenland. PhD Thesis, University of Birmingham, England.
- Herrington, P. M., and Fairchild, I. J., 1989. Carbonate shelf and slope facies evolution prior to Vendian glaciation, central East Greenland. In Gayer, R. A. (ed.), *The Caledonide Geology of Scandinavia*. London: Graham and Trotman, pp. 263–273.
- Hoffman, P.F., Halverson, G.P., Domack, E.W., Maloof, A.C., Swanson-Hysell, N.L., Cox, G.M., 2012. Cryogenian glaciations on the southern tropical paleomargin of Laurentia (NE Svalbard and East Greenland), and a primary origin for the upper Russøya (Islay) carbon isotope excursion. *Precambrian Research* 206, 137-158.
- Hoffman, P.F., Kaufman, A.J., Halverson, G.P., Schrag, D.P., 1998. A Neoproterozoic snowball earth. *Science* 281, 1342-1346.
- Irwin, H., Curtis, C., Coleman, M., 1977. Isotopic evidence for source of diagenetic carbonates formed during burial of organic-rich sediments. *Nature* 269, 209-213.
- Jahnert, R.J., Collins, L.B., 2012. Characteristics, distribution and morphogenesis of subtidal microbial systems in Shark Bay, Australia. *Marine Geology* 303, 115-136.
- Jiang, G., Kaufman, A.J., Christie-Blick, N., Zhang, S., Wu, H., 2007. Carbon isotope variability across the Ediacaran Yangtze platform in South China: Implications for a large surface-to-deep ocean $\delta^{13}\text{C}$ gradient. *Earth and Planetary Science Letters* 261, 303-320.
- Kennedy, M.J., Runnegar, B., Prave, A.R., Hoffmann, K.-H., Arthur, M.A., 1998. Two or four Neoproterozoic glaciations? *Geology* 26, 1059-1063.
- Klaebe, R., Kennedy, M., Jarrett, A., Brocks, J., 2017. Local paleoenvironmental controls on the carbon-isotope record defining the Bitter Springs Anomaly. *Geobiology* 15, 65-80.
- Knauth, L.P., Kennedy, M.J., 2009. The late Precambrian greening of the Earth. *Nature* 460, 728-732.
- Knoll, A., Hayes, J., Kaufman, A., Swett, K., Lambert, I., 1986. Secular variation in carbon isotope ratios from Upper Proterozoic successions of Svalbard and East Greenland. *Nature*, 832-838.
- Li, C., Hardisty, D.S., Luo, G., Huang, J., Algeo, T.J., Cheng, M., Shi, W., An, Z., Tong, J., Xie, S., Jiao, N., Lyons, T.W., 2017. Uncovering the spatial heterogeneity of Ediacaran carbon cycling. *Geobiology* 15, 211-224.
- Macdonald, F., Roots, C., 2009. Upper Fifteenmile Group in the Ogilvie Mountains and correlations of early Neoproterozoic strata in the northern Cordillera. *Yukon Exploration and Geology*, 237-252.
- Macdonald, F.A., Schmitz, M.D., Crowley, J.L., Roots, C.F., Jones, D.S., Maloof, A.C., Strauss, J.V., Cohen, P.A., Johnston, D.T., Schrag, D.P., 2010. Calibrating the Cryogenian. *Science* 327, 1241-1243.
- Meister, P., McKenzie, J., Warthmann, R., Vasconcelos, C., 2006. Mineralogy and petrography of diagenetic dolomite, Peru Margin, ODP Leg 201. *Proc. ODP Sci. Res.* 201.
- Melim, L.A., Swart, P.K., Maliva, R.G., 2001. Meteoric and marine-burial diagenesis in the subsurface of Great Bahama Bank, in: Ginsburg, R.N. (Ed.), *Subsurface Geology of a Prograding Carbonate Platform Margin, Great Bahama Bank*. SEPM Special Publication 70, 137–162.
- Moncrieff, A., Hambrey, M., 1990. Marginal-marine glacial sedimentation in the late Precambrian succession of East Greenland. Geological Society London, Special Publications 53, 387-410.

- Oehlert, A.M., Lamb-Wozniak, K.A., Devlin, Q.B., Mackenzie, G.J., Reijmer, J.J.G., Swart, P.K., 2012. The stable carbon isotopic composition of organic material in platform derived sediments: Implications for reconstructing the global carbon cycle. *Sedimentology* 59, 319-335.
- Prave, A., Fallick, A., Thomas, C., Graham, C., 2009. A composite C-isotope profile for the Neoproterozoic Dalradian Supergroup of Scotland and Ireland. *Journal of the Geological Society* 166, 845-857.
- Schrag, D.P., Berner, R.A., Hoffman, P.F., Halverson, G.P., 2002. On the initiation of a snowball Earth. *Geochemistry Geophysics Geosystems* 3.
- Schrag, D.P., Higgins, J.A., Macdonald, F.A., Johnston, D.T., 2013. Authigenic carbonate and the history of the global carbon cycle. *Science* 339, 540-543.
- Shields-Zhou, G., Hill, A., Macgabhann, B., 2012. The Cryogenian Period, in: Gradstein, F.M., Ogg, G., Schmitz, M. (Eds.), *The Geologic Time Scale*. Elsevier, 393-411.
- Sohl, L.E., Christie-Blick, N., Kent, D.V., 1999. Paleomagnetic polarity reversals in Marinoan (ca. 600 Ma) glacial deposits of Australia: Implications for the duration of low-latitude glaciation in Neoproterozoic time. *Geological Society of America Bulletin* 111, 1120-1139.
- Spence, G.H., Le Heron, D.P., Fairchild, I.J., 2016. Sedimentological perspectives on climatic, atmospheric and environmental change in the Neoproterozoic Era. *Sedimentology* 63, 253-306.
- Stouge, S., Christiansen, J.L., Harper, D.A., Houmark-Nielsen, M., Kristiansen, K., MacNiocaill, C., Buchardt-Westergård, B., 2011. Neoproterozoic (Cryogenian–Ediacaran) deposits in East and North-East Greenland. *Geological Society London, Memoirs* 36, 581-592.
- Swart, P.K., Eberli, G., 2005. The nature of the delta C-13 of periplatform sediments: Implications for stratigraphy and the global carbon cycle. *Sedimentary Geology* 175, 115-129.
- Sønderholm, M., Frederiksen, K.S., Smith, M.P., Tirsgaard, H., 2008. Neoproterozoic sedimentary basins with glacial deposits of the East Greenland Caledonides. *Geological Society of America Memoirs* 202, 99-136.
- Sønderholm, M., Tirsgaard, H., 1993. Lithostratigraphic framework of the Upper Proterozoic Eleonore Bay Supergroup of East and North-East Greenland. *Grønlands geologiske undersøgelse* 167.
- Tirsgaard, H., Sønderholm, M., 1997. Lithostratigraphy, sedimentary evolution and sequence stratigraphy of the Upper Proterozoic Lyell Land Group (Eleonore Bay Supergroup) of East and North-East Greenland. *Geology of Greenland Survey Bulletin* 178.
- Van Wagoner, J., Posamentier, H., Mitchum, R., Vail, P., Sarg, J., Loutit, T., Hardenbol, J., 1987. An overview of the fundamentals of sequence stratigraphy and key definitions, in: Wilgus, C., Posamentier, H., Van Wagoner, J., Ross, A., Kendall, C. (Eds.), *Sea-level changes: An integrated approach*. Society of Economic Paleontologists and Mineralogists Special Publication, pp. 109-124.
- Wang, W., Guan, C., Zhou, C., Peng, Y., Pratt, L.M., Chen, X., Chen, L., Chen, Z., Yuan, X., Xiao, S., 2017. Integrated carbon, sulfur, and nitrogen isotope chemostratigraphy of the Ediacaran Lantian Formation in South China: Spatial gradient, ocean redox oscillation, and fossil distribution. *Geobiology* 15, 552-571.
- Zhou, C., Guan, C., Cui, H., Ouyang, Q., Wang, W., 2016. Methane-derived authigenic carbonate from the lower Doushantuo Formation of South China: Implications for seawater sulfate concentration and global carbon cycle in the early Ediacaran ocean. *Palaeogeography, Palaeoclimatology, Palaeoecology* 461, 145-155.

Figure Captions

Figure 1. Compiled stratigraphic and carbon-isotopic correlation of the upper Andrée Land Group and a composite section constructed from the Backlundtoppen and Elbobreen formations (Russøya Member) in NE Svalbard following the conventional interpretation of Halverson (2007) and Hoffman et al. (2012). Here, the pre-Sturtian negative $\delta^{13}\text{C}$ excursion provides the basis for correlation between measured sections across NE Greenland and sections in Svalbard. This correlation relies on a subglacial surface (timeline #1) indicating the base of the Sturtian glaciation (Halverson et al., 2005; Hoffman et al., 2012) and two chemostratigraphic tie lines (timelines #2 and #3). The absence of positive $\delta^{13}\text{C}$ values below Sturtian glacial deposits in Svalbard and in southern regions of the NE Greenland Caledonides (Ella Ø) is attributed to sub-glacial erosion and truncation of the $\delta^{13}\text{C}$ curve by these authors, and is the focus of this study. Red shaded area indicates the negative $\delta^{13}\text{C}$ excursion. NE Svalbard stratigraphy and $\delta^{13}\text{C}$ data compiled from Halverson et al. (2004), Halverson et al. (2005) and Knoll et al. (1989). Kap Weber lithostratigraphy redrafted from Herrington and Fairchild (1989). Kap Weber $\delta^{13}\text{C}$ data measured in this study and was closely comparable with previously published data from Fairchild et al. (2000). Ella Ø section and $\delta^{13}\text{C}$ data measured in this study.

Figure 2. Study Area. a) Simplified geological map of North-East Greenland (central fjord zone) showing the sediments of the Neoproterozoic Eleonore Bay Basin. Field sections are at Kap Weber (northern star, base at approximately 73° 30.000'N 25° 5.000'W) and Ella Ø (southern star, base at 72° 52.885'N 25° 7.697'W). Modified from Søndersholm et al. (2008) after Henriksen (2003) and Bengaard (1991). b) Map of Neoproterozoic deposits on Ella Ø after Fairchild et al. (2000). Bed-group 19 measured section locations are indicated by arrows. c) Generalised stratigraphy of the upper Eleonore Bay Supergroup and overlying Tillite Group modified after Søndersholm et al. (2008).

Figure 3. Representative lithofacies in bed-group 18 on Ella Ø. a) Channelised pisolitic and microspar carbonate from lower bed-group 18. Diffuse boundaries between pisoid allochems and overlying microsparite indicates that much of the preserved sparry limestones here are destructively recrystallised allochems. b) Chert nodules in bed-group 18 microsparite. Chert preserves original pisolitic textures of the sediment that is now homogeneous structureless microspar. c) Intraformational carbonate conglomerates from bed-group 18. Matrix-supported poorly sorted (dolomitic) conglomerate with diverse limestone and dolostone clasts (peloids, bladed mud-clasts, subrounded pebbles). Individual conglomerate beds are 0.25 to 1 m thick and are commonly associated with stromatolite bioherms and microbial mats. d) Up to 5 m thick cumulate stromatolite domes capping the first major shallowing cycle in bed-group 18. Each dome shows several growth stages in cross-section from discrete 1-3 cm domes nucleated on an intraclastic substrate through radially distributed columnar forms that coalesce as metre-scale, interconnected bioherms. e) Dolomitised columnar stromatolites, bed-group 18. f) Upper bed-group 18 dolomitic karst-collapse breccia with 1 to 2 cm thick fibrous dolospar interstitial cements.

Figure 4. Representative lithofacies of bed-group 19 from Ella Ø. a) 4th order shallowing cycles in lower bed-group 19. Basal mudstones (red) transition up-section into interbedded then stacked fine-grained, dolomite-rich turbidite sequences. b) Typical carbonate-poor mudstone from bed-group 19. c) Packages of mm-scale distal turbidite sequences (current lamination and massive hemipelagic cap couplets), middle bed-group 19. d) Channelised tabular-clast slope debrite, middle bed-group 19.

Figure 5. Summary of cyclic sedimentation in bed-group 19 from Storeelv and Kløftelv sections on Ella Ø. Cycles 1-3 correspond to lower three cycles generalised in Figure 12. Flooding surfaces are indicated by sharp vertical transitions from coarser stacked distal turbidite facies and/or clastic debrites to deeper-water massive to finely laminated mudstones.

Figure 6. Backscatter electron (BSE) images of bed-group 19 mudstones showing the distribution of framboidal and euhedral pyrite a) Pyrite (bright spots) concentrated along discrete bedding-parallel lenses. b) Close-up image of pyrite showing that it occurs as framboids and as individual euhedral crystals that are disseminated throughout mudstone matrix.

Figure 7. Basal contact between upper bed-group 19 and the Ulvesø Formation on Ella Ø. a) Sharply channelised diamictite embedded into the uppermost mudstone beds of bed-group 19, Tommerbugt. Base of continuous diamictite indicated by dashed line, arrows point to lenses of diamictite embedded in upper mudstone beds of bed-group 19. b) Plane-polarised thin section image of channelised diamictite in upper bed-group 19 with visible mud stringer. c) Mudstone stringers (arrows) incorporated into the lower ~5 m of the Ulvesø Formation at Tommerbugt. Mud stringers are elongate, discontinuous and approximately bedding parallel with underlying mudstones. d) Thin section image of lower Ulvesø Formation diamictite from Tommerbugt. Clast composition is dominated by subrounded quartz and calcite microspar. e) Large scale flame-structure at the base of Ulvesø Formation diamictites, Ella Ø. f-g) Concave-up limestone structures within the lower ~10 m of Ulvesø Formation diamictites at Klostelv (dashed lines in f). These lens-shaped bodies are > 95% carbonate and are dominantly calcitic compared to the dolomitic carbonate cements dominating surrounding diamictite. h) Thin section image of relict allochems (likely ooids) in basal Ulvesø Formation limestone lenses. Some grains are partially dolomitised at their margins. i) Composite schematic sketch of the basal Ulvesø Formation on Ella Ø, illustrating the intimately interbedded and conformable nature of the contact. Mudstones are shaded dark-grey, limestone rafts in light grey, diamictites and clasts are not shaded.

Figure 8. Scatter plot of $\delta^{13}\text{C}$ versus $\delta^{18}\text{O}$ values from bed-group 18, bed-group 19 and the basal Ulvesø Formation (Ella Ø), and bed-group 20 (Kap Weber).

Figure 9. BSE and energy dispersive spectrometric (EDS) map of massive mudstone from bed-group 19, Ella Ø. Sample from 9m above the base of bed-group 19 siliciclastic sediments. a) Backscatter image of typical carbonate-poor mudstone from lower bed-group 19 at Storeelv. b) 3-element EDS image showing distribution of dolomite (cyan) versus siliciclastic minerals in the same sample. Spot analysis reveals that the cyan minerals are dolomite, red are quartz, green are calcite, and purple are mixtures of (berthierine) clay and mica. Quartz grains are finer than most dolomite rhombs and are less angular. > 4 μm dolomite grains do not preserve rhombic crystal shape and are thus likely to be detrital and similar in origin to well-rounded detrital limestone (green). Red = Si, Green = Ca, Blue = Mg.

Figure 10. BSE and EDS maps of laminated mudstone 72m above base of bed-group 19 siliciclastic rocks on Ella Ø. a) BSE image of laminated mudstone, bed-group 19. b) Fe map highlighting clay laminae in sample. Clay minerals (versus quartz) defines sub-millimetre laminae throughout sample. c) Ca map showing coarse calcitic cements (white) and coarse dolomite rhombs (grey). Microspar-grade carbonate does not follow depositional layering of clay minerals versus coarser siliciclastics. d) 3-element EDS image. Spot analysis confirms that cyan grains are dolomite, red are quartz, purple are clays and green material is calcite. Dolomite occurs as coarse euhedral crystals evenly distributed throughout samples and as > 4 μm grains (dolomicrite)

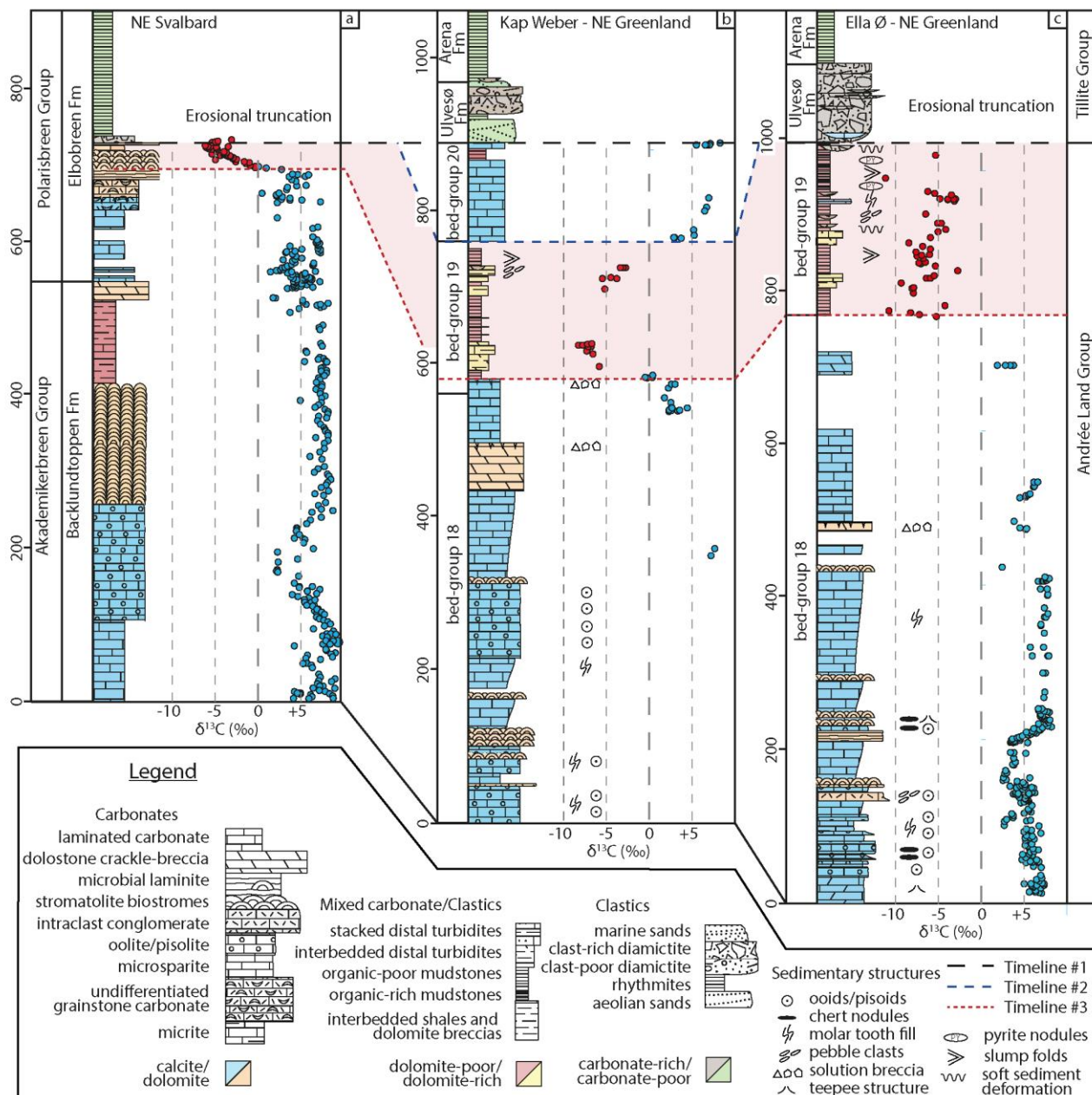
that occur within clay rich horizons. Dolomite rhombs appear to displace siliciclastic grains while calcite fills space between quartz grains and euhedral dolomite. Red = Si, Green = Ca, Blue = Mg. e) Close-up of Ca map showing dolomite rhombs overgrown by calcite (black box in panel d). Fine detrital dolomite grains are visible in the top-left corner.

Figure 11. EDS maps of distal turbidite, 89 m above base of bed-group 19 siliciclastics on Ella Ø. a) 3-element EDS map of coarse siliciclastic turbidite base cutting the dolomite-rich hemipelagic cap of the previous cycle. Arrows point to top of the bed. Red = Si, Green = Ca, Blue = Al. b) Ca map showing distribution of dolomite grain size. While siliciclastic grains are well sorted depending on position in the cycle, coarse dolomite rhombs are evenly disseminated throughout the cycle and show no sorting. Dolomicrite is more abundant in the hemipelagic cap (bottom-right).

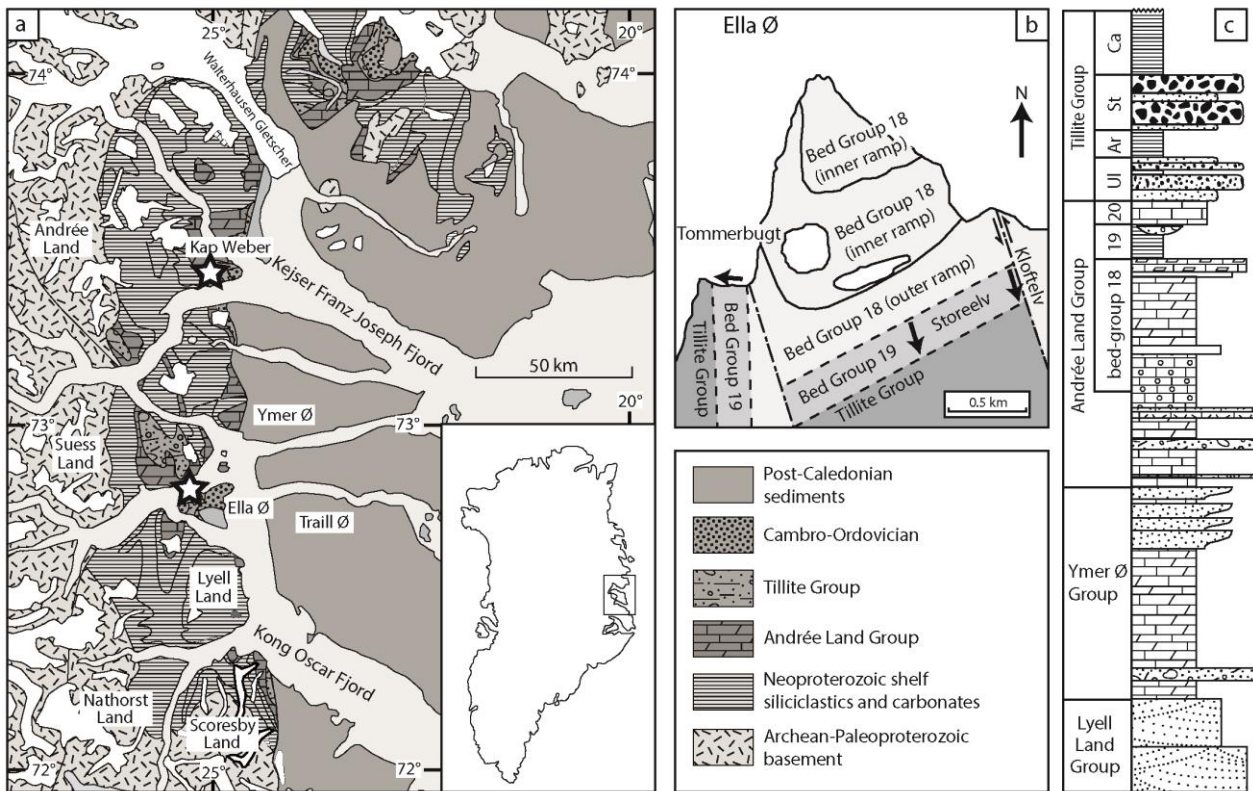
Figure 12. Stratigraphic correlation of the Ella Ø and Kap Weber field sections (Fairchild et al. 2000). Sequence boundaries are marked with dashed lines. a-f correspond to the panels Figure 13. Calibration of the two sections relies on a regional flooding surface at the base of bed-group 19 mudstones and the erosion surface (Kap Weber) and correlative conformity (Ella Ø) at the base of the Ulvesø Formation. Correlations between these surfaces are based on sharp vertical transitions between coarser slope turbidites (yellow) and debris flows (brown), and basin massive and laminated mudstones (red), or in the upper interval of Kap Weber outer ramp carbonates (blue) and basin mudstones (red).

Figure 13. Basin evolution model for the upper Andrée Land Group. Arrow indicates direction of sea-level change compared to previous panel. Relative position of measured sections at Kap Weber and Ella Ø shoreline indicated by vertical lines on panels.

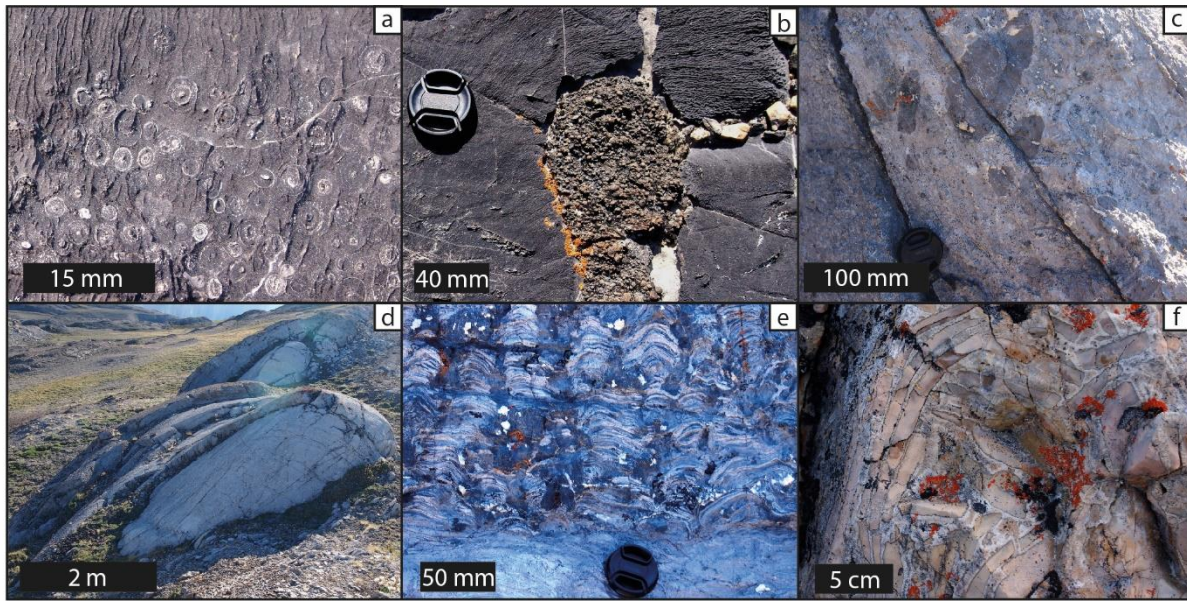
Figure 14. The Kap Weber and Ella Ø stratigraphic and $\delta^{13}\text{C}$ chemostratigraphic profiles superimposed onto the basin evolution model presented in Figure 13. Stratigraphic logs are height-corrected to account for lateral thickness variation of facies belts.



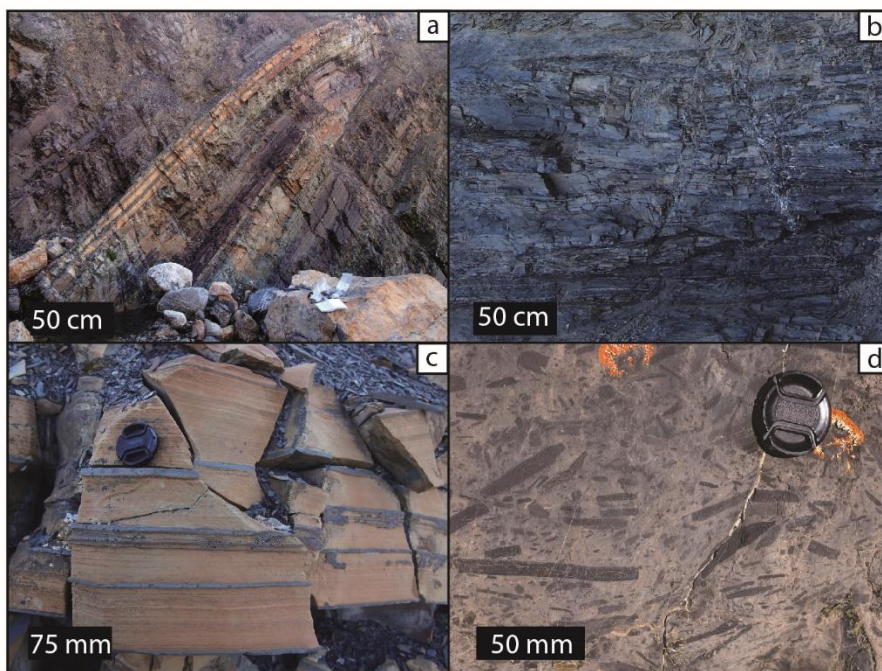
Klaebe et al. Figure 1



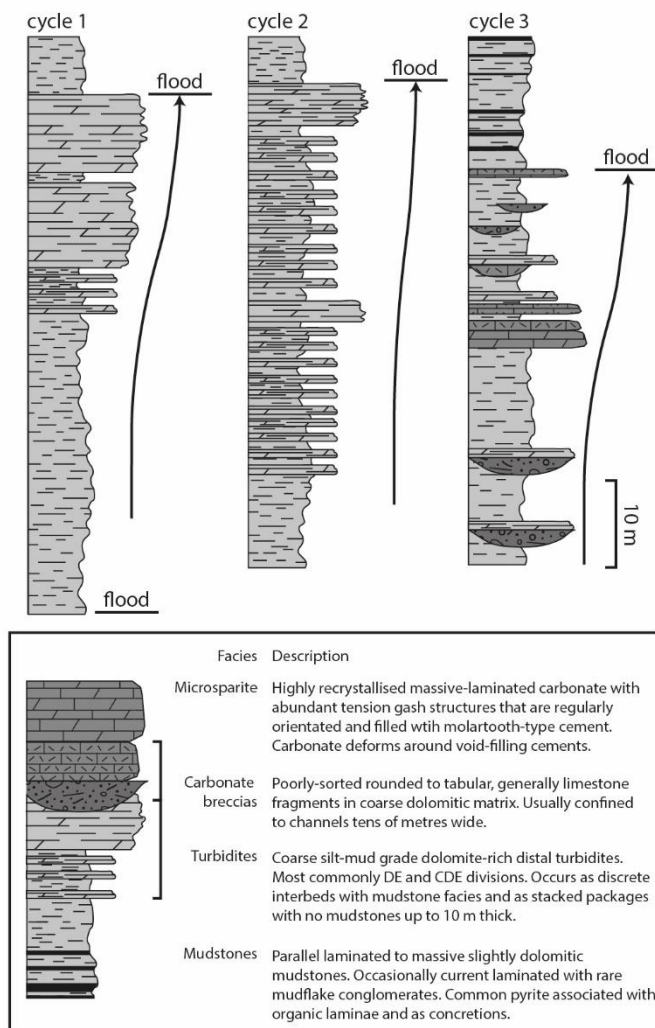
Klaebe et al. Figure 2



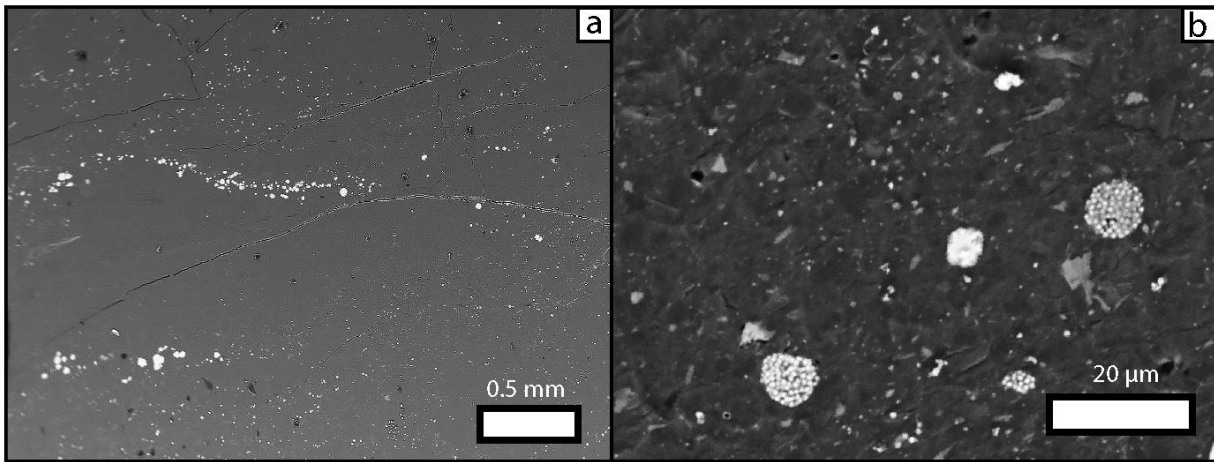
Klaebe et al. Figure 3



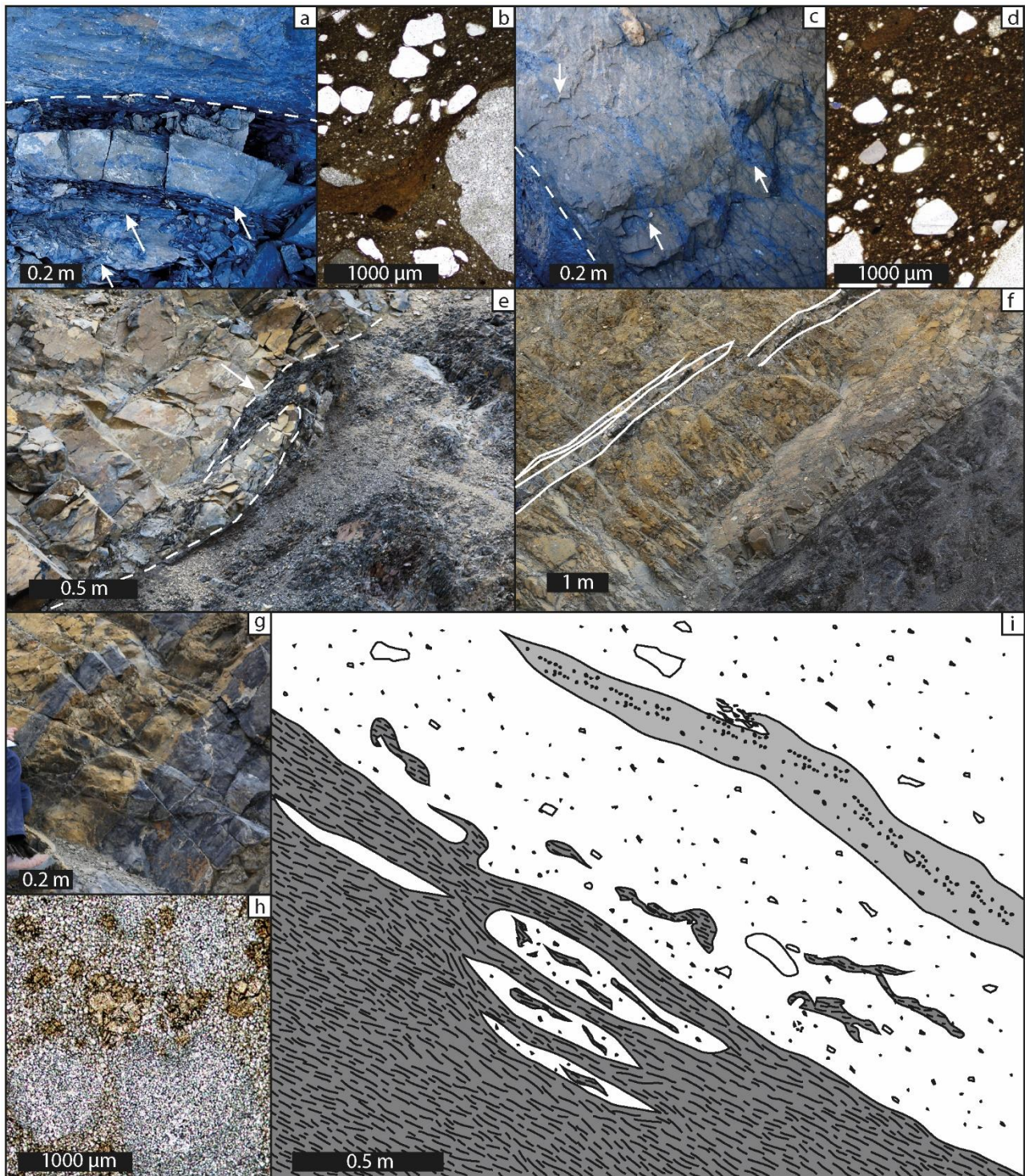
Klaebe et al. Figure 4



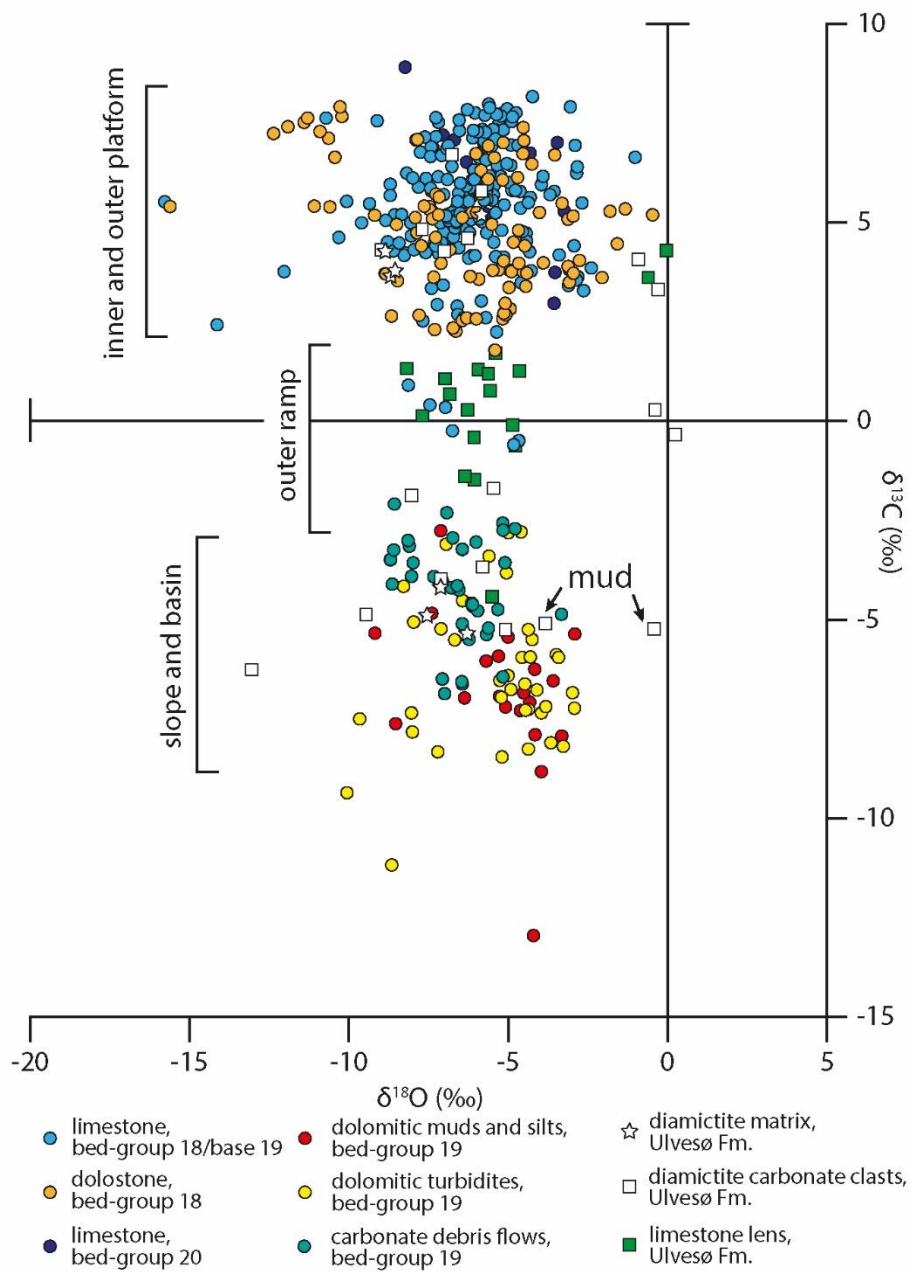
Klaebe et al. Figure 5



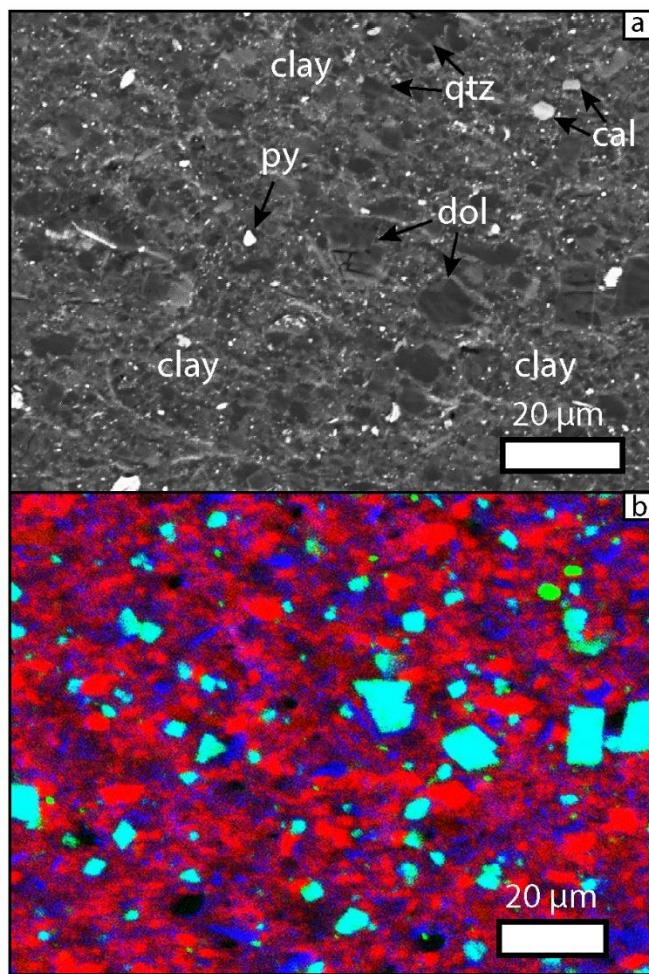
Klaebe et al. Figure 6



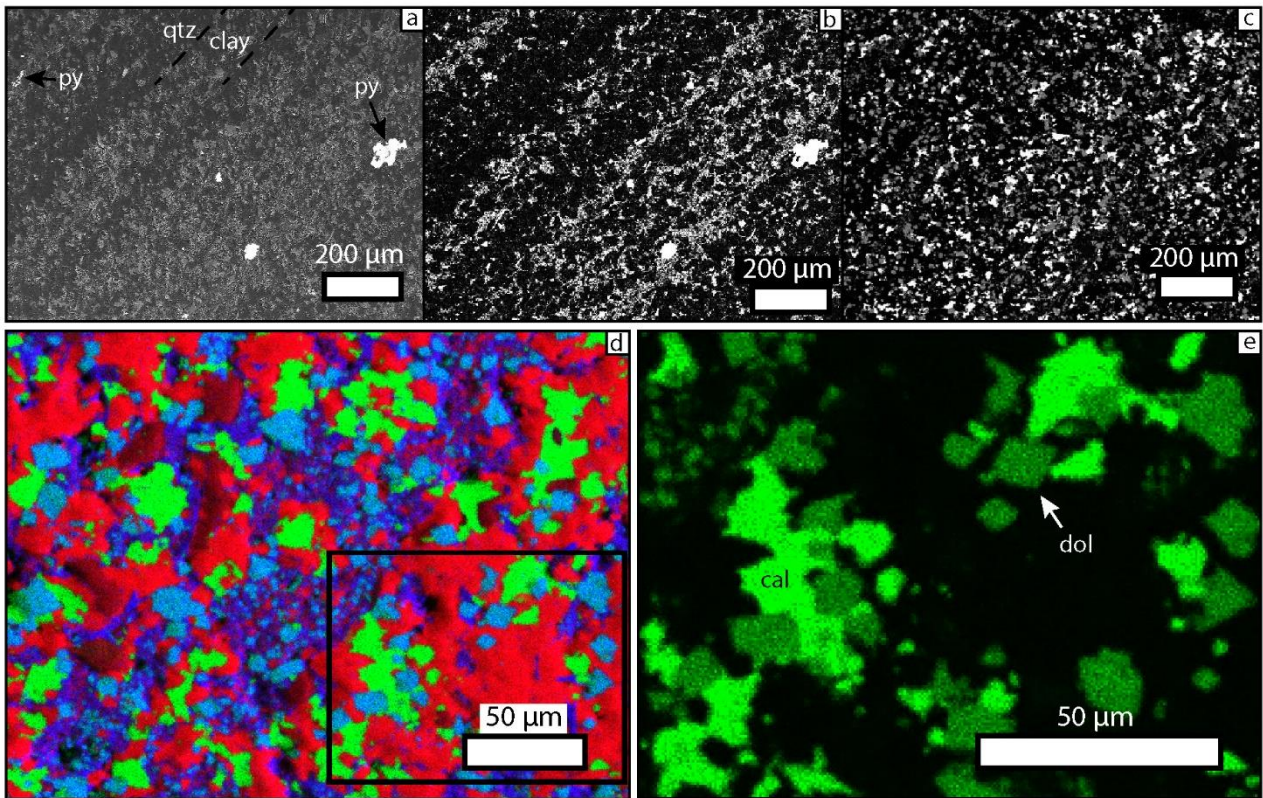
Klaebe et al. Figure 7



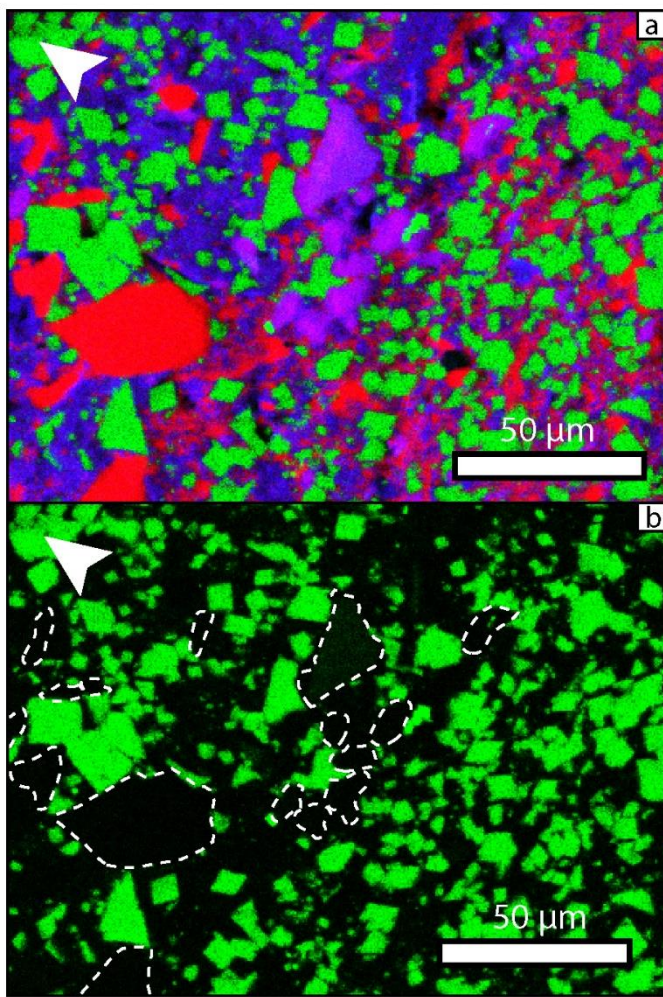
Klaebe et al. Figure 8



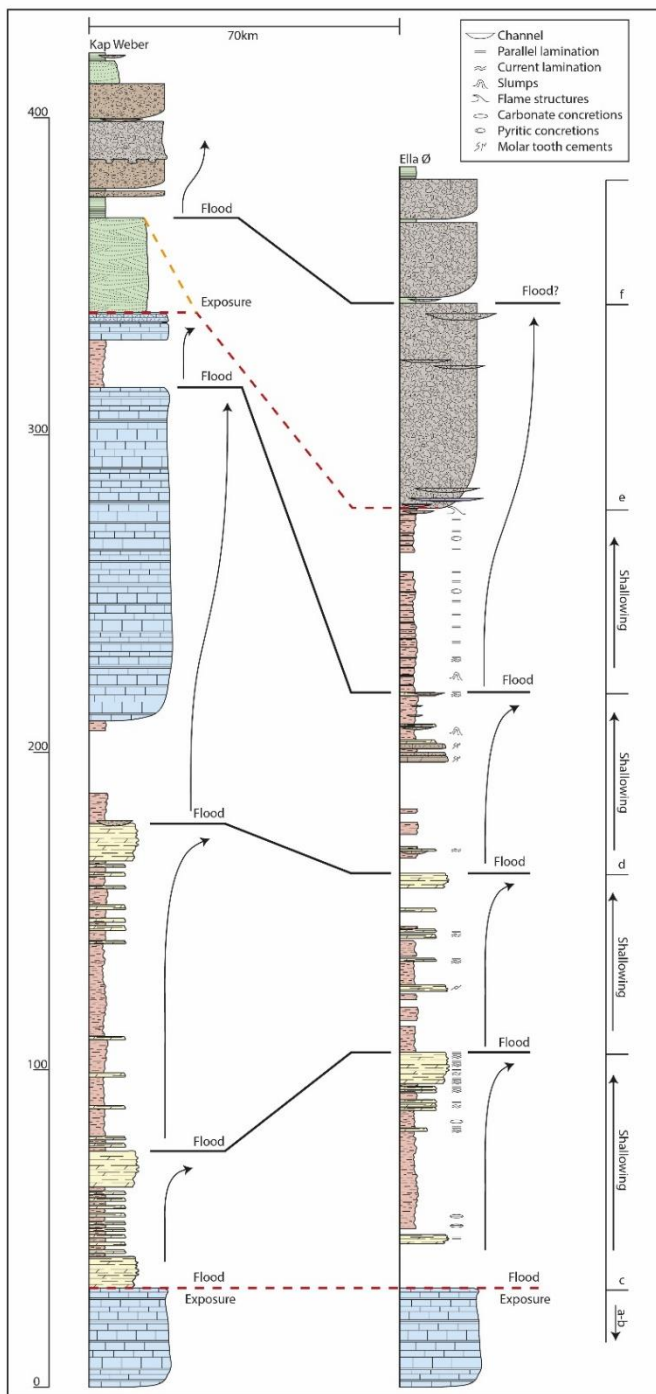
Klaebe et al. Figure 9



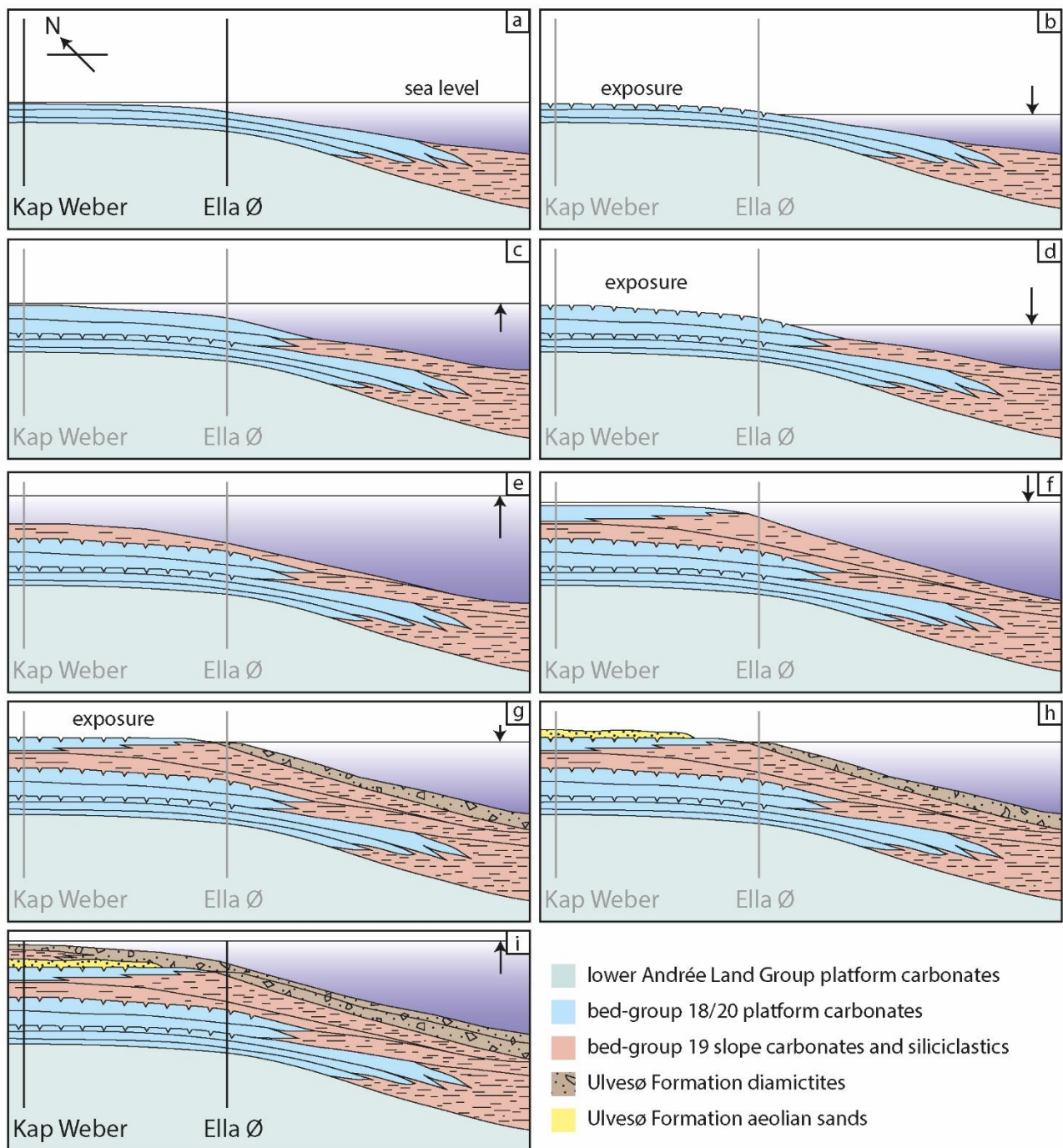
Klaebe et al. Figure 10



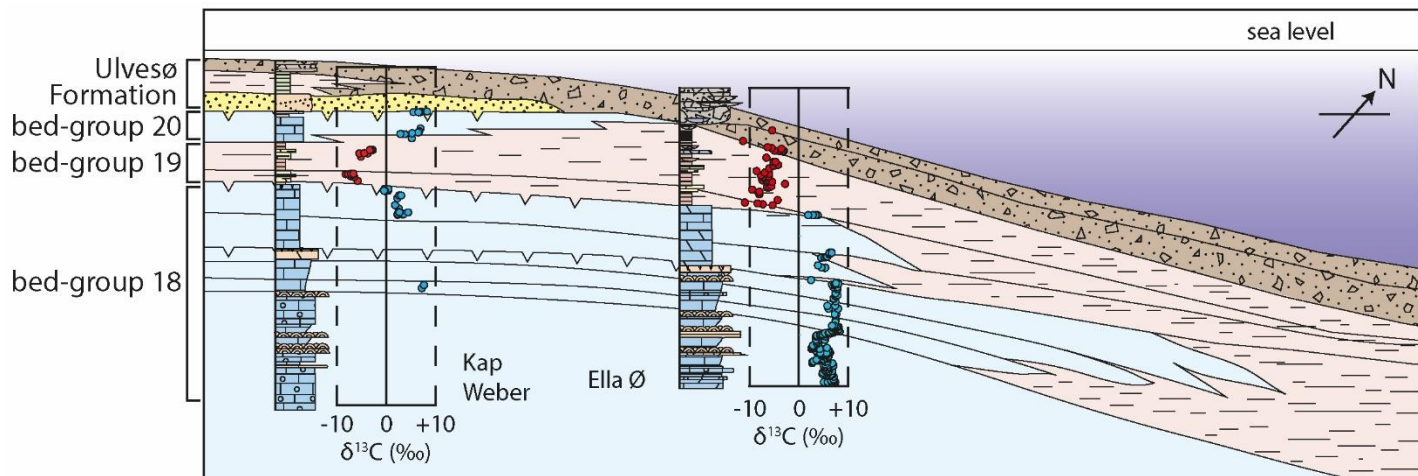
Klaebe et al. Figure 11



Klaebe et al. Figure 12



Klaebe et al. Figure 13



Klaebe et al. Figure 14